Article

Cell Reports

# Drug-induced eRF1 degradation promotes readthrough and reveals a new branch of ribosome quality control

## Graphical abstract

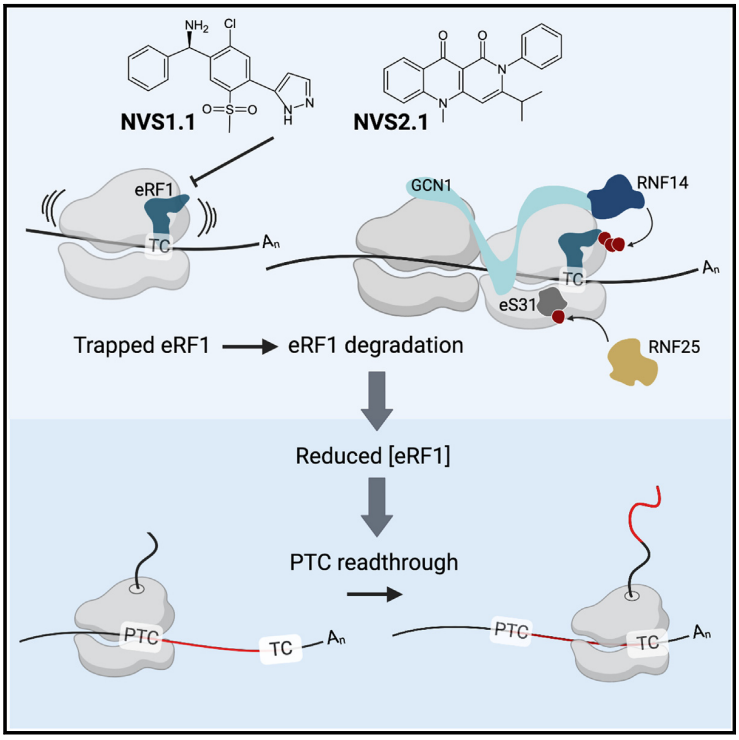


## Highlights

- NVS1.1 and NVS2.1 restore CFTR and IDUA activity in CF and Hurler disease models
- The drugs induce proteasomal eRF1 degradation and readthrough of PTCs
- And block translation termination by trapping eRF1 in the A site, causing ribosome collisions
- GCN1, RNF14, and RNF25 sense occluded A sites and degrade the trapped eRF1

## Authors

Lukas-Adrian Gurzeler, Marion Link, Yvonne Ibig, ..., Niko Schmiedeberg, Oliver Mühlemann, Jürgen Reinhardt

## Correspondence

oliver.muehlemann@unibe.ch (O.M.), juergen.reinhardt@novartis.com (J.R.)

## In brief

Gurzeler et al. present two potent readthrough promoters, NVS1.1 and NVS2.1, that restore functional full-length proteins in cystic fibrosis and Hurler disease models. These compounds promote readthrough of premature termination codons by triggering eRF1 degradation by a ribosome-associated quality control pathway involving GCN1, RNF14, and RNF25.

Gurzeler et al., 2023, Cell Reports *42*, 113056
September 26, 2023 
https://doi.org/10.1016/j.celrep.2023.113056

CellPress

Cell Reports

CellPress
OPEN ACCESS

Article

# Drug-induced eRF1 degradation promotes readthrough and reveals a new branch of ribosome quality control

Lukas-Adrian Gurzeler,[1,2] Marion Link,[3] Yvonne Ibig,[3] Isabel Schmidt,[3] Olaf Galuba,[3] Julian Schoenbett,[3] Christelle Gasser-Didierlaurant,[3] Christian N. Parker,[3] Xiaohong Mao,[4] Francis Bitsch,[3] Markus Schirle,[4] Philipp Couttet,[3] Frederic Sigoillot,[4] Jana Ziegelmüller,[1,2] Anne-Christine Uldry,[5] Wojciech Teodorowicz,[1,2] Niko Schmiedeberg,[3] Oliver Mühlemann,[1,6,*] and Jürgen Reinhardt[3,*]

[1]Department of Chemistry, Biochemistry and Pharmaceutical Sciences, University of Bern, Bern, Switzerland
[2]Graduate School for Cellular and Biomedical Sciences, University of Bern, Bern, Switzerland
[3]Novartis Institutes for BioMedical Research, Basel, Switzerland
[4]Novartis Institutes for BioMedical Research, Cambridge, MA, USA
[5]Proteomics and Mass Spectrometry Core Facility, Department for BioMedical Research, University of Bern, Bern, Switzerland
[6]Lead contact
*Correspondence: oliver.muehlemann@unibe.ch (O.M.), juergen.reinhardt@novartis.com (J.R.)
https://doi.org/10.1016/j.celrep.2023.113056

## SUMMARY

Suppression of premature termination codons (PTCs) by translational readthrough is a promising strategy to treat a wide variety of severe genetic diseases caused by nonsense mutations. Here, we present two potent readthrough promoters—NVS1.1 and NVS2.1—that restore substantial levels of functional full-length CFTR and IDUA proteins in disease models for cystic fibrosis and Hurler syndrome, respectively. In contrast to other readthrough promoters that affect stop codon decoding, the NVS compounds stimulate PTC suppression by triggering rapid proteasomal degradation of the translation termination factor eRF1. Our results show that this occurs by trapping eRF1 in the terminating ribosome, causing ribosome stalls and subsequent ribosome collisions, and activating a branch of the ribosome-associated quality control network, which involves the translational stress sensor GCN1 and the catalytic activity of the E3 ubiquitin ligases RNF14 and RNF25.

## INTRODUCTION

About 10% of known genetic diseases result from nonsense mutations that prematurely truncate the coding sequence (CDS).[1] Examples include CFTR, IDUA, and dystrophin mutations, which cause cystic fibrosis (CF), Hurler syndrome (mucopolysaccharidosis type I, MPS I), and Duchenne muscular dystrophy, respectively.[2–4] Promoting translational readthrough at premature termination codons (PTCs) is a promising therapeutic strategy to produce functional full-length protein. Several small molecules were developed and tested in recent years to suppress nonsense codon recognition and increase PTC readthrough frequency.[4] For instance, geneticin (G-418), an aminoglycoside, induces readthrough of termination codons (TCs) and has been evaluated in various disease models.[5,6] Although clinical trials indicated the production of some full-length functional protein and chemically synthesized aminoglycoside variants even showed reduced ototoxicity and kidney liabilities, the clinical application of aminoglycosides as readthrough drugs is under debate.[3,7] Non-aminoglycoside readthrough promoters, including Ataluren (previously PTC-124[8]) and the anti-allergic drug Amlexanox,[9] have been identified through multiple screens. Nevertheless, the currently available readthrough promoters have shown modest and controversial clinical performance, emphasizing the need for better readthrough-promoting drugs.

During translation termination, when a ribosome encounters a TC (UAA, UAG, or UGA), a ternary complex consisting of the eukaryotic release factor 1 (eRF1) (also known as eukaryotic termination factor 1 [ETF1]) and the GTP-bound GTPase eRF3 (also known as GSPT1) binds to the aminoacyl-tRNA site (A site). After eRF3-mediated GTP hydrolysis, eRF1 assumes its catalytically active conformation and cleaves the peptidyl-tRNA bond of the peptidyl-tRNA located in the ribosome's P site.[10–12] This triggers a rotation between the ribosomal subunits, leading to the release of the free polypeptide and eRF1, ultimately resulting in the splitting and recycling of the ribosomal subunits.[13] Under normal conditions, translation termination is fast and highly accurate. Readthrough, which involves the incorporation of a near-cognate aminoacyl-tRNA, occurs in <0.1% of termination events and depends on the TC and its surrounding sequence context.[14] Interestingly, readthrough appears to happen more frequently at disease-associated PTCs than at physiological TCs (>1%; Manuvakhova et al.[15]), presenting an opportunity for pharmacologically induced PTC-specific readthrough.[16] While the mode of action of most readthrough-promoting agents remains unknown, aminoglycosides reduce the accuracy of ribosomal decoding,

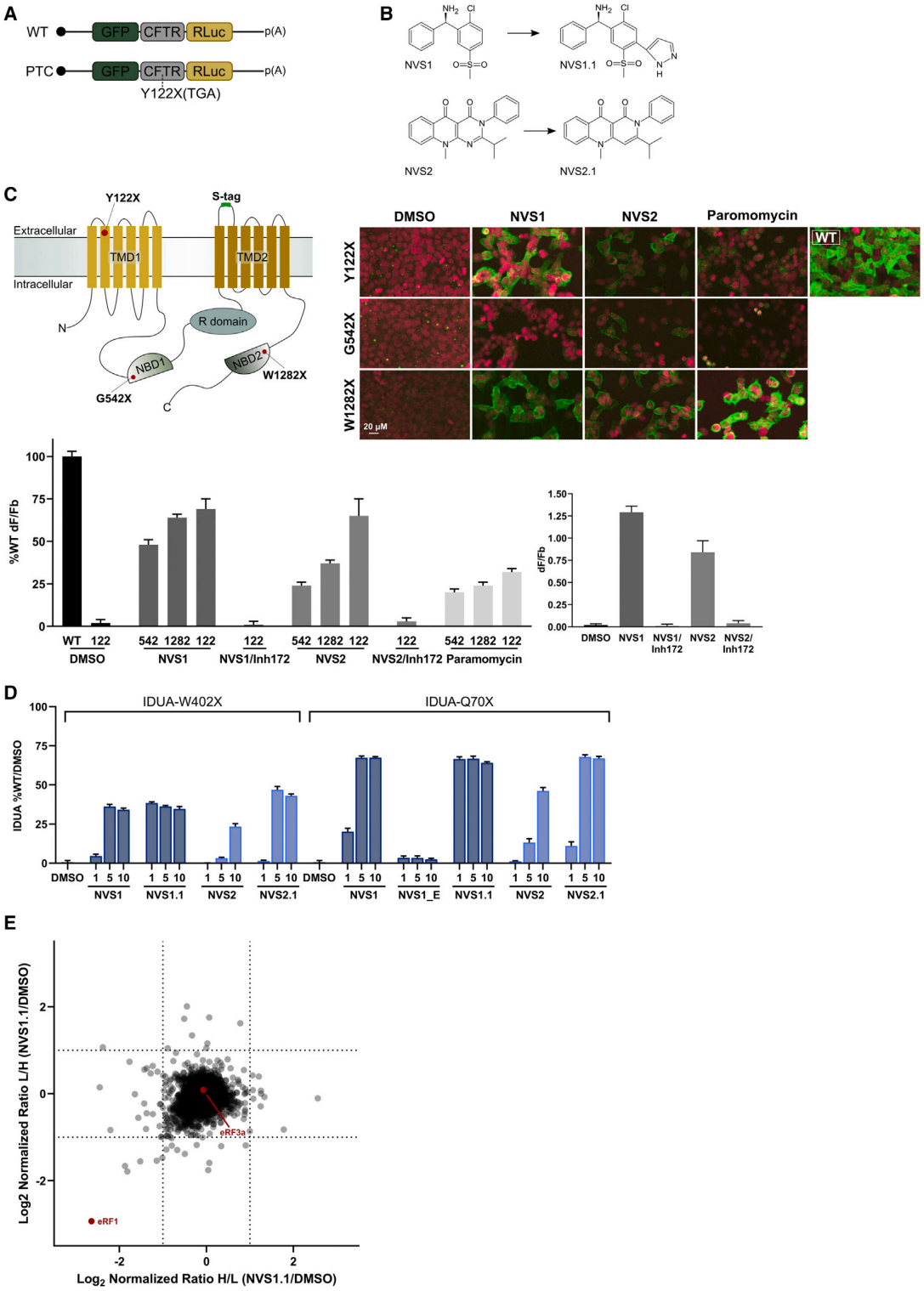


(legend on next page)

thereby increasing the probability of a near-cognate tRNA pairing with a TC in the A site and promoting translation beyond the TC.[5] Another mechanism involves limiting the concentrations of eRF1 and eRF3, which slows down termination and increases the chances of near-cognate tRNA binding to ribosomes halted at TCs.[17] However, depleting release factors has not been exploited as a therapeutic approach to promote readthrough.

Here, we present the identification and pharmacological optimization of two small-molecule compounds with distinct chemical scaffolds that enhance translational readthrough by inducing rapid degradation of eRF1. Both molecules mediate substantial readthrough in disease-relevant recombinant and primary cell models of CF and Hurler syndrome. Encouraging proof-of-concept studies in a rat model of MPS I Hurler syndrome highlight their therapeutic potential. Mechanistic investigations reveal that these compounds trap eRF1 in the A site of ribosomes, thereby inhibiting translation termination and causing ribosome collisions. Our work uncovers a cellular translational quality control mechanism that recognizes and clears occluded A sites through ubiquitination and rapid proteasomal degradation of eRF1. This pathway involves GCN1 and the two ubiquitin ligases RNF14 and RNF25. The resulting decrease in cellular eRF1 concentration explains the observed increase in PTC readthrough in cells treated with the compounds.

## RESULTS

### High-throughput screen identifies potent readthrough-promoting compounds

To screen for small molecules promoting readthrough at PTCs, we used a reporter construct comprising a 60 bp region of the CFTR CDS with a nonsense mutation at codon 122 (Y122X, position corresponds to full-length CFTR) fused in-frame between an N-terminal GFP and a C-terminal *Renilla* luciferase (RLuc) CDS (Figure 1A). This readthrough reporter was integrated into the pre-engineered R4 site of the Jump-In HEK293 cell line (referred to as HEKR4) and constitutively expressed. The resulting HEKR4 PTC reporter cells were used for a high-throughput primary screen in which $1.6 \times 10^6$ compounds were scored for causing increased RLuc activity. A total of 21,645 compounds increased RLuc activity to >35% of the activity observed with the aminoglycoside paromomycin, which was used as the positive reference compound (Figure S1A). These hits were further tested in a confirmation screen carried out in triplicate. In addition, a CFTR-WT reporter construct (Figure 1A) expressed in HEKR4 cells was used to eliminate false positive hits that increased RLuc activity in a PTC-independent manner. The confirmation and filter screens derived 5,198 active hits, of which 3,038 were validated by assessing dose-response curves (Figure S1A). The candidates were further tested in HEKR4 cells expressing a full-length version of the human coagulation factor 9 enzyme with a nonsense mutation at amino acid position 29 (Figure S1A). At this stage, two scaffolds named NVS1 and NVS2 (Figure 1B) were prioritized and further validated using cellular models for CF (CFTR, Figure 1C) and Hurler syndrome (IDUA, Figure 1D). Confocal imaging of non-permeabilized cells using an antibody detecting an inserted surface epitope (S-tag; Novagen) in the fourth extracellular loop of CFTR[18] showed that NVS1 and NVS2 restored full-length CFTR expression at the cell membrane, with more CFTR resulting from readthrough of the UAA at position 122 and the UAG at position 1,282 than of the UGA at position 542 (Figure 1C, upper right). To assess the functionality of the restored full-length protein, we conducted a forskolin-stimulated CFTR membrane potential assay after compound treatment. Consistent with the imaging results, NVS1 and NVS2 promoted readthrough most efficiently on the Y122X mutant, followed by W1282X and G548X, respectively (Figure 1C, lower panels). Both compounds were superior to the readthrough-promoting control compound paromomycin. Furthermore, co-administration of the CFTR inhibitor Inh172[19] abolished the NVS1- and NVS2-mediated membrane potential depolarization, demonstrating that both compounds restore functional CFTR activity in the CFTR-Y122X cell model.

Next, HEKR4 cells expressing IDUA-Q70X and IDUA-W402X were used for structure-activity relationship guided compound optimization. A total of 179 derivatives of NVS1 and NVS2 were synthesized and compared for their ability to restore IDUA enzyme activity. Of those, the diphenylmethanamine derivate NVS1.1 and the pyrimido(4,5-B)quinoline-4,5(3H,10H)-dione NVS2.1 (Figure 1B; Novartis patents WO2014/091446A1 and WO2015/186063A1) were selected for further testing (Figure 1D). The

**Figure 1. High-throughput screen identifies small molecules stimulating PTC readthrough in recombinant cell models**

(A) Schematic of the readthrough reporter mRNA used for screening. The GFP, a CFTR fragment with or without the PTC mutation (Y122X) and the RLuc CDS were fused in-frame.

(B) Chemical structures of the molecules NVS1, NVS2, NVS1.1, and NVS2.1.

(C) CFTR expression restoration and chloride channel activity in HEKR4 cells with CFTR nonsense mutations. Upper left: schematic of CFTR depicting transmembrane (TMD), nucleotide-binding (NBD), and regulatory (R) domains and the tested nonsense mutations. The extracellular S-tag allows detection of correctly inserted CFTR into the cell membrane. Upper right: cells expressing the indicated CFTR mutants were treated with 12.5 μM NVS1, 50 μM NVS2, or 10 mM paromomycin for 48 h. Wild-type (WT) CFTR-expressing cells served as positive control. Non-permeabilized cells were incubated with the anti-S-tag antibody (green) and nuclei were stained with DRAQ5 (red). Lower left: CFTR chloride channel activity measurements in cells expressing the indicated CFTR nonsense mutants pre-treated with 10 μM NVS1 or NVS2, or 10 mM paromomycin, for 48 h before stimulation with 20 μM forskolin. Percentages of the activity in untreated WT CFTR-expressing cells are shown. Lower right: CFTR activity after addition of 10 μM of the CFTR chloride channel blocker 172 for 20 min in the presence of NVS1 or NVS2. Mean values ± SD are shown.

(D) Restoration of α-L-iduronidase activity in HEKR4 cells expressing IDUA Q70X and W402X mutants treated with 1, 5, or 10 μM of the indicated compounds for 48 h. NVS1_E is the inactive enantiomer of NVS1. Enzymatic activities are displayed as percentage of IDUA activity in untreated cells expressing WT IDUA. Mean values ± SD are shown.

(E) Proteome changes induced by NVS1.1 in HEKR4 cells were monitored by SILAC-MS analysis. The experiment was performed twice, once by labeling the NVS1.1-treated cells with the heavy isotope (H) and the DMSO-treated cells with the light isotope (L), and once with inverted isotope labeling. The $\log_2$ of the normalized H/L or L/H ratios for each detected protein is plotted.

chemically optimized molecules NVS1.1 and NVS2.1 outperformed the HTS-derived compounds NVS1 and NVS2 in potency, with superior IDUA activity restoration in both the Q70X and the W402X cell models. Neither DMSO nor treatment with an inactive enantiomer of NVS1 (NVS1_E) restored detectable IDUA enzyme activity. Liquid chromatography followed by mass spectrometry-based peptide analysis of NVS1.1, NVS2.1, and paromomycin-treated IDUA-W402X cell lines showed glutamine (Q) being preferentially incorporated at UAG nonsense codons and tryptophan (W) at UGA, while UAA led to the incorporation of tyrosine (Y), glutamine (Q), or lysine (K) (Figure S1B), similar to a previous report in yeast showing that nonsense suppression occurs by use of near-cognate tRNAs.[20]

To further characterize NVS1.1, we assessed proteome alterations upon stimulation of translational readthrough by performing quantitative proteomic profiling using stable isotope labeling by amino acids in cell culture (SILAC)[21] in parental HEKR4 cells either incubated with NVS1.1 or DMSO (negative control). The SILAC experiment was repeated with reversed isotope labeling of the two conditions, and the abundance ratio between the NVS1.1-treated and the control sample was determined for each protein detected in both experiments (Figure 1E; Table S1). Remarkably, we observed a specific 6.5- to 7-fold reduction of eRF1 upon NVS1.1 treatment in both experiments, suggesting that NVS1.1 promotes the rapid and specific degradation of eRF1. Since the reduction of translation termination efficiency by the depletion of eukaryotic release factors leads to stop codon suppression,[22–24] the finding that NVS1.1 causes reduced eRF1 levels explains its readthrough-promoting activity. Whereas it was shown that eRF3 degradation results in co-depletion of eRF1,[22,25] we observed no effect of NVS1.1 on eRF3 abundance, indicating that eRF3 stability is not regulated by eRF1 levels (Figure 1E).

Immunoblotting confirmed the NVS1.1-induced eRF1 depletion and showed that NVS2.1 also reduces eRF1 levels (Figure S1C), suggesting that both compounds might promote translational readthrough by similar mechanisms, despite of being structurally unrelated. Consistent with our findings, another derivative of NVS2, covered by the Novartis patents WO2014/091446A1 and WO2015/186063A1 and named SRI-41315, was recently also reported to promote readthrough by triggering eRF1 degradation, but its mode of action remained unexplored.[26]

## NVS1.1 and NVS2.1 restore synthesis of α-L-iduronidase in primary fibroblast of Hurler syndrome patients

To determine the therapeutic potential of NVS1.1 and NVS2.1, we tested them in primary fibroblasts derived from Hurler syndrome patients with homozygous mutations in the IDUA gene. Reduced α-L-iduronidase (IDUA) activity, a glycosidase involved in the breakdown of glycosaminoglycans (GAG), causes a spectrum of disorders collectively referred to as mucopolysaccharidosis type I (MPS I) and disease burden correlates with residual α-L-iduronidase activity.[27,28] Hurler syndrome represents the most severe form of MPS I, exhibits complete α-L-iduronidase deficiency, and leads to death in early childhood. The most frequently found mutations in Hurler syndrome are the homozygous nonsense mutations W402X[UAG] and Q70X[UAG], which were used in recombinant cell models to optimize our readthrough promoters.[28] The patient-derived primary fibroblasts lack detectable α-L-iduronidase activity and consequently accumulate large amounts of GAG in an increased number of enlarged lysosomal compartments.[29] Being the rate-limiting enzyme in lysosomal GAG processing, already small amounts of restored α-L-iduronidase activity can clear the cellular GAG overload and attenuate disease severity.[30–32] In our patient cells homozygous for the W402X mutation, treatment for 7 days with NVS1.1 (Figure 2A) or NVS2.1 (Figure S2A) caused a dose-dependent increase of IDUA activity, accompanied by a GAG reduction. Because loss of function mutations of IDUA were shown to upregulate other genes involved in GAG degradation,[33] we monitored the activity of the hydrolase β-glucuronidase (GUSB). Concomitant with the depletion of GAG, we observed a >2-fold reduction of GUSB activity, indicating that the NVS1.1-mediated IDUA restoration stabilizes the GAG degradation pathway (Figure 2A). An even more pronounced dose-dependent increase of IDUA activity occurred with NVS1.1 and NVS2.1 in patient-derived fibroblasts homozygous for the Q70X mutation (Figure S2B).

Since translational readthrough of PTCs can inhibit the degradation of nonsense mRNAs by the nonsense-mediated mRNA decay (NMD) pathway,[34] we tested if NVS1.1 inhibits NMD of the IDUA-W402X mRNA. qRT-PCR time-course experiments in the IDUA-W402X fibroblasts showed that up to 2 μM NVS1.1, IDUA mRNA levels remained essentially unchanged, while it increased over time with 5 μM NVS1.1 (Figures 2B and S2C). Since we observed increased IDUA activity at NVS1.1 concentrations <1 μM, the observed increase in IDUA protein and enzymatic activity originates primarily from translational readthrough and is not the result of higher mRNA levels due to NMD inhibition.

Next, we tested long-term administration of the drugs and found that treatment of the IDUA-W402X fibroblasts with NVS1.1 or NVS2.1 for 7 weeks also restored IDUA activity (Figures 2C and S2D). Importantly, for both compounds the dose-dependent restoration of IDUA activity correlated with the extent of eRF1 depletion and GAG reduction. Treatment with 0.6 μM NVS1.1 reduced GAG, the most disease-relevant parameter, to half compared with untreated fibroblasts (Figure 2C), and 2 μM NVS2.1 reduced the accumulated GAG by 80% (Figure S2D). These results indicate that NVS1.1 or NVS2.1 might have therapeutic potential for treating Hurler syndrome.

## NVS1.1 is efficacious in a rat Hurler IDUA-W401X animal model

For proof-of-concept studies, a rat model for Hurler syndrome homozygous for the W401X mutation in the IDUA gene was engineered, mirroring the human disease-linked W402X mutation. To verify responsiveness of the animal model to our compounds, we isolated skin fibroblasts and treated them for 7 days with NVS1.1 and NVS2.1. As in the human patient-derived fibroblasts, both compounds restored IDUA enzyme activity and reduced the GAG levels in a dose-dependent manner (Figures 3A and S3A), demonstrating that the IDUA-W401X rat model qualifies to investigate the *in vivo* efficacy of NVS1.1 and NVS2.1. The soluble NVS1.1 compound showed good drug-like properties with favorable pharmacokinetics, metabolic stability, and suitability for oral administration. Acceptable profiles for oral

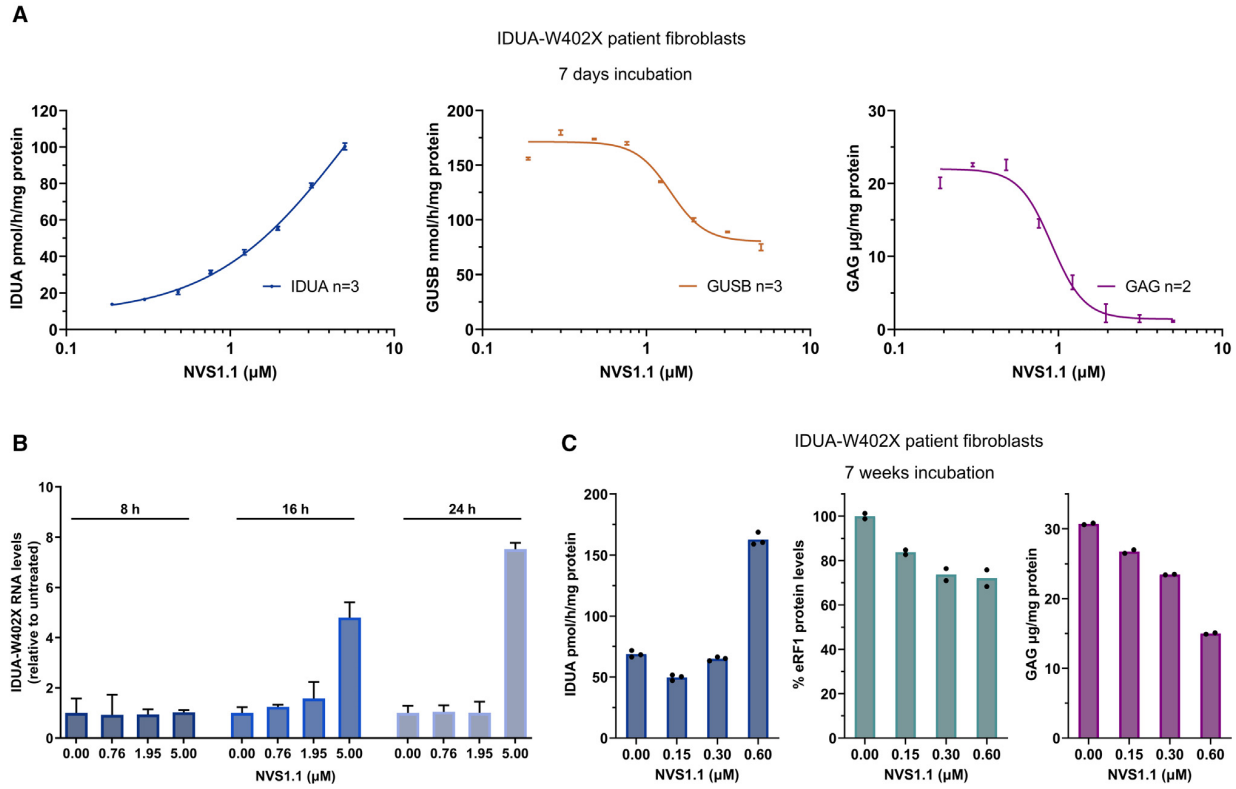


**Figure 2. NVS1.1 restores α-L-iduronidase in Hurler patient-derived fibroblasts**

(A) Primary fibroblasts from patients homozygous for the IDUA W402X mutation were treated with the indicated NVS1.1 concentrations for 7 days, and α-L-iduronidase (IDUA) and β-glucuronidase (GUSB) activities were measured. Total glycosaminoglycan levels were determined and normalized to total protein abundance (GAG, μg/mg protein). Mean values ± SD are shown.

(B) qRT-PCR measurements of the IDUA-W402X mRNA levels upon treatment of the Hurler primary fibroblasts with different concentrations of NVS1.1 for 8–24 h. IDUA mRNA levels were normalized to GAPDH and shown relative to the vehicle-treated control condition for each time point. Mean values ± SD are shown (n = 3).

(C) Long-term treatment of Hurler patient fibroblasts with the indicated concentrations of NVS1.1. After 7 weeks, IDUA activity (left panel) and total GAG levels (right panel) were determined as in (A). eRF1 protein abundance (middle panel) was assessed by immunoblot (using β-actin as a loading control) and is shown relative to the DMSO control condition. Bars depict mean values and black dots represent the values of biological replicates.

*in vivo* pharmacology studies were derived for NVS2.1, too. Current therapeutic interventions for Hurler patients focus on enzyme replacement and hemopoietic stem cell transplantation (HSCT). Although HSCT can ameliorate neurological phenotypes if applied at an early age (1–1.5 years), it is accompanied with inherent safety risks. Therefore, alternative (co-)treatment options addressing the brain defects are needed and brain-penetrable readthrough compounds would represent a promising addition to the current standard care for MPS I patients carrying nonsense mutations. To investigate brain exposure of NVS1.1 and NVS2.1, we determined their concentrations in the rat cerebrospinal fluid (CSF) after a single orally administered drug dose of 10 mg/kg and compared it with the concentrations found in blood and free plasma (Figures 3B and S3B). Both compounds resulted in similar concentrations in the CSF as in the plasma and this ratio remained stable over time, showing that both compounds efficiently reach the brain.

Our initial *in vivo* efficacy studies therefore focused on IDUA restoration and biomarker responses in rat brain tissue. Hurler rats were treated with NVS1.1 or NVS2.1, and brain tissues were then analyzed for restored IDUA enzyme activity, GUSB enzyme response, and total GAG levels as described above. Daily oral dosing for 14 days with 40 mg/kg body weight NVS1.1 and NVS2.1 significantly restored IDUA enzyme activity and reduced the GAG load, whereas the 20 mg/kg dosing for both compounds showed clear but not statistically significant restoration effects (Figures 3C and S3C). Both 40 mg/kg doses of NVS1.1 and NVS2.1 restored approximately 1% of the IDUA activity measured in brain tissue of untreated WT rats, resulting in a GAG reduction by 36% and 57% in the brains of Hurler rats treated with 20 and 40 mg/kg NVS1.1, and by 50% with 40 mg/kg NVS2.1, respectively. Interestingly, as in the patient-derived fibroblasts (Figures 2A and S2A), the GUSB enzyme activity increased by more than 2-fold in the Hurler rats compared with WT rats, but was dose dependently reduced by NVS1.1 and NVS2.1, reaching approximately 1.3-fold of WT rats with both compounds dosed at 40 mg/kg (Figures 3C and S3C). Collectively,

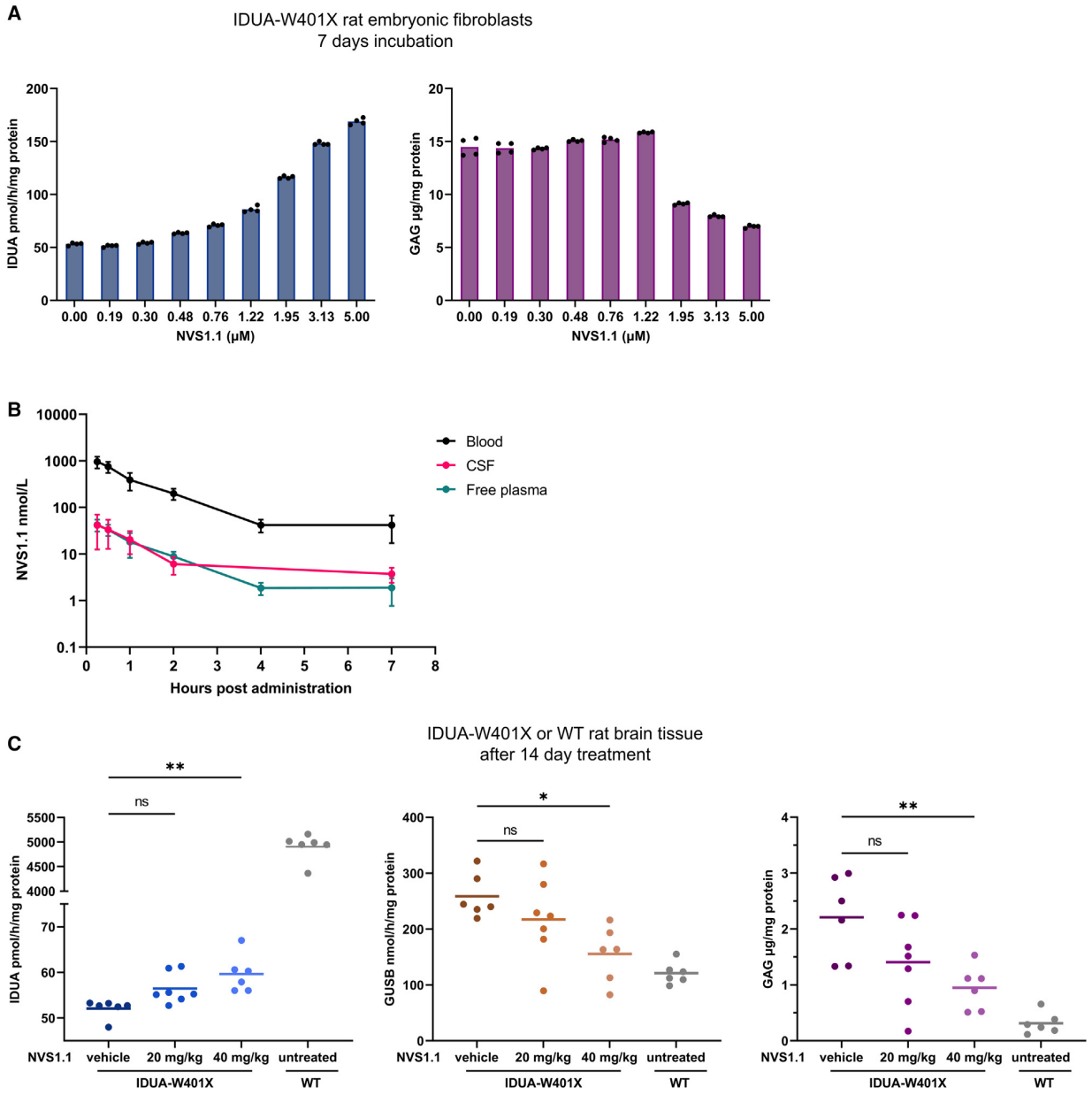


**Figure 3. NVS1.1 reduces the glucosamine load in the brain of a rat Hurler disease model**

(A) Effects of NVS1.1 treatment on IDUA enzyme activity and total GAG levels in freshly isolated rat fibroblasts homozygous for IDUA-W401X. IDUA activity and total GAG levels were determined as in Figure 2A.

(B) NVS1.1 concentrations in total blood, cerebrospinal fluid (CSF), and free plasma at different time points after a single oral administration of 10 mg/kg NVS1.1 to male Sprague-Dawley rats (n = 3). Mean values ± SD are shown.

(C) IDUA and GUSB activity, and total GAG levels in the brain of NVS1.1-treated Hurler rats and untreated IDUA-WT rats. After 14 days, IDUA and GUSB activities and total GAG levels were determined as in Figure 2A from extracted brain tissue. One dot represents the average of four technical replicates carried out with brain tissue from one animal. p values were calculated by one-way ANOVA followed by Dunnet's multiple comparisons test. *$p \leq 0.05$, **$p \leq 0.01$, $p > 0.05$, ns, respectively.

our data suggest that the pharmacologically optimized molecules NVS1.1 and NVS2.1 restore IDUA sufficiently to clear the cellular GAG levels *in vivo* within 2 weeks of oral administration in the Hurler rat model.

## NVS1.1 induces ubiquitination of eRF1 on K279, leading to proteasomal eRF1 degradation

Assessing the changes in the proteome upon treatment with NVS1.1 identified a specific and substantial depletion of eRF1

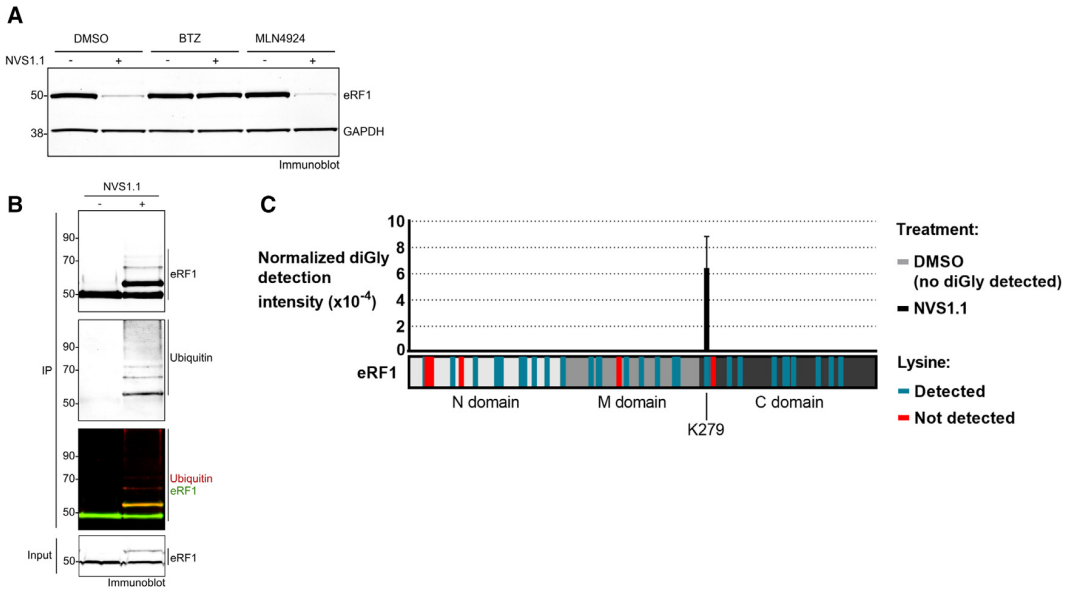


**Figure 4. NVS1.1 induces proteasomal degradation of eRF1 via ubiquitination of K279**

(A) Protein levels of eRF1 in HEKR4 PTC reporter cells after treatment with 2.5 μM NVS1.1 for 6 h in the presence of DMSO, 0.5 μM proteasome inhibitor bortezomib (BTZ), or 1 μM neddylation inhibitor MLN4924. GAPDH served as a loading control.

(B) Ubiquitination analysis of eRF1 in HeLa cells treated with 25 μM NVS1.1 for 30 min eRF1 was immunoprecipitated and the eluates were analyzed by immunoblotting for eRF1 and ubiquitin.

(C) Ubiquitination sites in eRF1 detected by mass spectrometry from immunoprecipitates in (A). To detect ubiquitination sites, the trypsin-digested eRF1 peptides were inspected for glycine-glycine (diGly) remnants on lysine residues. The x axis shows the eRF1 protein sequence with its domain organization, positions of lysine-containing peptides detected in at least two replicates in each of the two conditions are depicted in blue, not detected peptides in red. The averaged diGly signal intensity obtained from the modified peptide intensities detected in NVS1.1 is shown as black bar and was normalized by their respective protein intensities (y axis).

(Figure 1E), providing a mechanistic explanation for the readthrough-promoting activity of the NVS1.1. Canonical protein decay occurs via the proteasome, which recognizes and degrades proteins marked with polyubiquitin. Co-treatment of cells with NVS1.1 and the proteasome inhibitor bortezomib fully stabilized eRF1, indicating that NVS1.1-induced eRF1 depletion occurs by proteasomal degradation (Figure 4A). To investigate whether NVS1.1 induces eRF1 ubiquitination, we immunoprecipitated eRF1 from cells treated with a high dose (25 μM) of NVS1.1 for a short time (30 min) to capture modified eRF1 before its degradation. Subsequently, we performed immunoblot analysis with antibodies against eRF1 and ubiquitin (Figure 4B). Demonstrating NVS1.1-mediated eRF1 ubiquitination, mono-, bi-, and tri-ubiquitinated eRF1 was detected in the NVS1.1-treated cells but not in the control sample. The eRF1 immunoprecipitates were also analyzed by label-free mass spectrometry, which showed a strong enrichment of ubiquitin upon treatment of the cells with NVS1.1 (Figure S4; Table S2). Furthermore, analysis of peptides with di-glycine (diGly) remnants conjugated to the epsilon amino group of lysines (K), which allows the identification of ubiquitination sites in a protein,[35] identified K279 of eRF1 as the main site for NVS1.1-induced ubiquitination (Figure 4C; Table S2).

Since numerous previously identified small-molecule degraders modulate the receptor specificity of Cullin-RING ligase 4 (CRL4), we addressed if NVS1.1 employs a similar mechanism. CRL4 ligases require neddylation for their activation,[36–38] which can be prevented by the neddylation inhibitor MLN4924. However, NVS1.1-induced eRF1 depletion was not inhibited by the co-treatment of the cells with MLN4924 (Figure 4A), indicating that NVS1.1 is not a molecular glue degrader that employs CRL4 E3 ligases, but instead has a different mode of action.

## NVS1.1-mediated eRF1 degradation requires the E3 ligases RNF14 and RNF25

To identify ubiquitin ligases involved in the NVS1.1-dependent ubiquitination of eRF1, we employed two orthogonal approaches, a genome-wide CRISPR knockout (KO) screen scoring for cells that survive under high NVS1.1 concentrations and a genome-wide siRNA screen scoring for reduced readthrough of the *Renilla* luciferase readthrough reporter in cells exposed to NVS1.1. Both screens independently revealed the two E3 ubiquitin-protein ligases RNF14 (UniProt: Q9UBS8) and RNF25 (UniProt: Q96BH1) as top hits (Figure 5A; Table S3). Both proteins contain RING finger domains typical for E3 ubiquitin ligases, but little is known about the function and ubiquitination targets of RNF14 and RNF25. RNF14 was reported to be a membrane bound E3 ubiquitin ligase that is associated with the androgen receptor and acts as a co-activator of its transcriptional activity[39,40] and a regulator of TCF/β-catenin-mediated transcription.[41] RNF25 has been shown to support NF-κB-mediated transcription by interacting with its p65 subunit.[42]

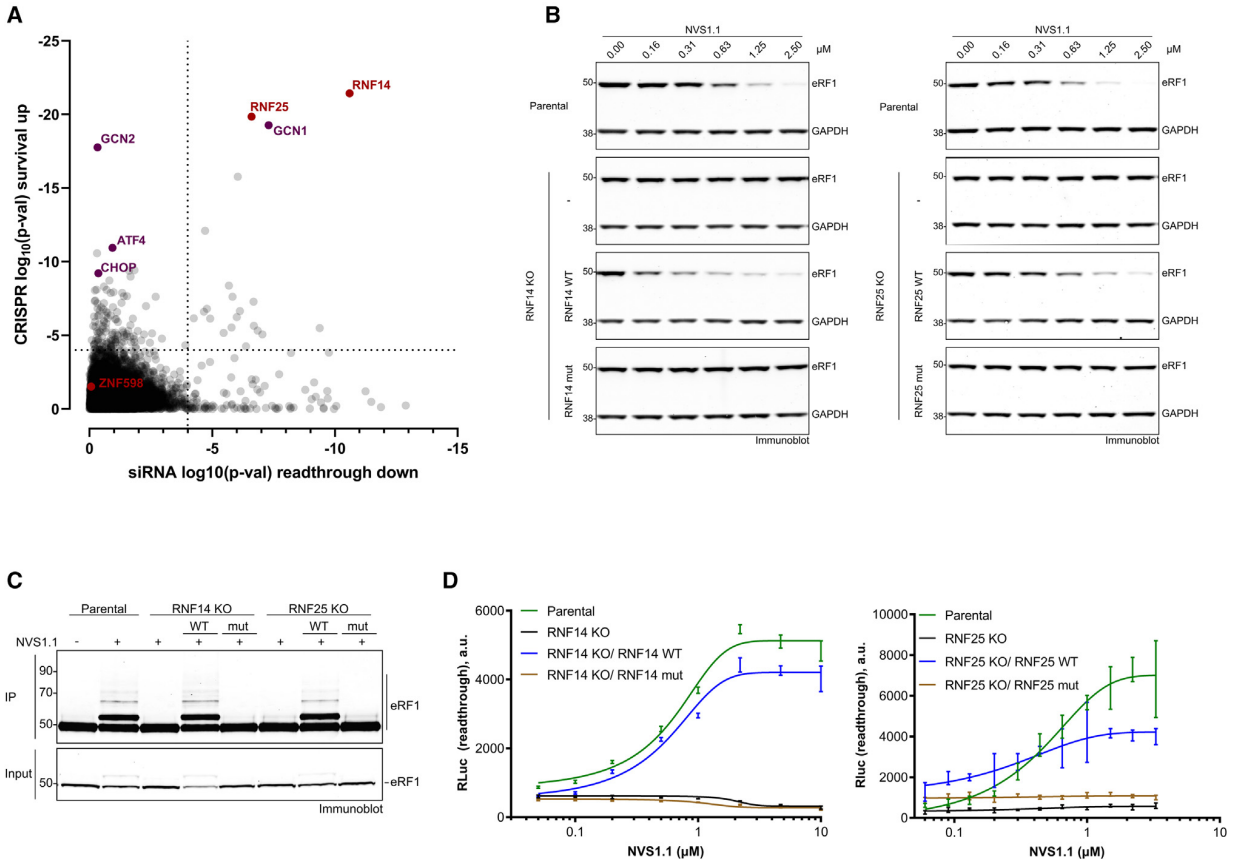


**Figure 5. NVS1.1-mediated eRF1 degradation depends on catalytically active E3 ligases RNF14 and RNF25**

(A) Combined results of genome-wide siRNA and CRISPR screens for genes affecting NVS1.1 activity. x axis: $\log_{10}$ p values of inhibition of NVS1.1-induced CFTR-Y122X-Rluc reporter readthrough in HEKR4 cells for the knockdown of each tested gene (8 siRNAs per gene). Rluc activity was normalized to the signal of a non-targeting siRNA ($\log_2$FC) and the difference between the NVS1.1 $IC_{80}$ versus DMSO conditions was determined. The significance for the differential activity of each knockdown was calculated using RSA statistical test (redundance siRNA activity).[43] y axis: $\log_{10}$ p values for reverting NVS1.1-induced toxicity in a cell survival assay for the knockout of each tested gene. Differential representation of each sgRNA in NVS1.1 $IC_{80}$ and untreated library-infected cell populations was determined as surrogate of difference in cell proliferation. Gene significance was calculated for the differential representation of each sgRNA set (five sgRNAs per gene) using the RSA statistical test. For both screens, significance thresholds were determined by randomizing the gene labels before running the RSA tests. A $\log_{10}$(p-val) <-4 threshold (dotted lines) limited false positives to ~5%.

(B) Effects of RNF14 and RNF25 knockouts (KO) and rescue on eRF1 levels and ubiquitination in HEKR4 PTC reporter cells. Rescue cell lines stably overexpress either the wild-type (WT) protein or a catalytically inactive mutant (RNF14mut [C220S] and RNF25mut [C135S/C138S], respectively). Parental, KO, and rescue cells were incubated with the indicated NVS1.1 concentrations for 6 h. eRF1 levels cells were assessed by immunoblotting, GAPDH was used as a loading control.

(C) Ubiquitination status of eRF1 in the parental, KO, and rescue cells after incubation with 25 μM NVS1.1 for 30 min. Following eRF1 immunoprecipitation, 50% of the eluates and 1% of input were analyzed by immunoblotting using anti-eRF1 antibody.

(D) Translational readthrough measurements (represented as arbitrary units [a.u.]) in parental, KO, and rescue cells after incubation with a serial dilution of NVS1.1 for 24 h. Mean values ± SD are shown.

To validate the involvement of RNF14 and RNF25 in NVS1.1-induced eRF1 degradation, we generated clonal knockouts of these genes in the HEKR4 PTC reporter cells and tested the sensitivity of eRF1 for NVS1.1-induced degradation (Figures 5B and S5A). While, in the parental cells, eRF1 protein levels were decreased in a dose-dependent manner, the KO of RNF14 or RNF25 rendered the cells resistant to NVS1.1-induced eRF1 degradation. Complementation analysis showed that the NVS1.1 sensitivity was restored by the expression of recombinant active RNF14 (WT) but not by a catalytically inactive RNF14 RING finger domain mutant (C220S)[44] (Figures 5B and S5A). Likewise, RNF25 WT but not the catalytically inactive RNF25 mut (C135S/C138S)[45] restored NVS1.1 sensitivity of eRF1 in the RNF25 KO cells (Figures 5B and S5A).

eRF1 ubiquitination was only detected in cells expressing active RNF14 and RNF25 but not in cells depleted for one of the two E3 ligases or in cells expressing mutated versions of either RNF14 or RNF25, demonstrating that RNF14 and RNF25 are non-redundant and both required for ubiquitinating eRF1 in response to NVS1.1 (Figure 5C). The absence of ubiquitinated

eRF1 upon KO of either E3 ligase excludes a scenario in which one factor catalyzes the mono-ubiquitination and the other E3 ligase extends ubiquitin chains. Consistent with the requirement of RNF14 and RNF25 for eRF1 degradation, both E3 ligases also proved essential for NVS1.1-induced readthrough (Figure 5D). Readthrough of the PTC of the RLuc reporter gene (Figure 1A) increased in a NVS1.1 dose-dependent manner in parental cells and in cells in which the KO of RNF14 or RNF25 was rescued by overexpressing the respective WT proteins. In the RNF14 and RNF25 KO cells overexpressing the respective mutant proteins, only background luminescence was detected, suggesting that they are not responsive to the readthrough molecule (Figure 5D). Collectively, this demonstrates that the extent of NVS1.1-induced readthrough directly depends on the intracellular concentration of eRF1, which is regulated by RNF14 and RNF25.

Despite being chemically distinct from NVS1.1, the mode of action of NVS2.1 appears to be identical: the siRNA and CRISPR screens conducted with NVS2.1 also identified RNF14 and RNF25, albeit the latter did not pass the threshold filter in the siRNA screen (Figure S5B; Table S3).

### NVS1.1 triggers a GCN1-mediated ribosome-associated quality control by trapping eRF1 on terminating ribosomes

In addition to RNF14 and RNF25, the CRISPR screen revealed GCN1, GCN2 (also known as EIF2AK4), ATF4, and CHOP as top hits (Figure 5A). GCN1 is a positive regulator of the protein kinase GCN2, which is implicated in the activation of the integrated stress response (ISR), leading to the inhibition of translation initiation by phosphorylation of eIF2-$\alpha$. This global protein synthesis repression is accompanied by the upregulation of ATF4 and other stress response factors.[46–48] Depending on the intensity and duration of ISR, different cellular fates ensue, ranging from pro-survival signaling promoting cellular recovery during short-lived stresses, to programmed cell death upon sustained ISR.[47] It is therefore plausible that, during eRF1 depletion, loss of ISR factors increased cell survival by delaying apoptosis, conferring indirectly NVS1.1 resistance to these cells in the CRISPR screen. A similar observation was found for CC-90009, a molecular glue degrader triggering the depletion of eRF3A.[37] However, in contrast to the other identified ISR factors, GCN1 was additionally strongly enriched in the siRNA screen, which scored for readthrough inhibition (Figure 5A), arguing for a direct role of GCN1 in the NVS1.1-triggered eRF1 degradation. Indeed, GCN1 knockdown caused a marked stabilization of eRF1 in the presence of NVS1.1 (Figure 6A). Therefore, we conclude that GCN1 is a key component of the pathway by which NVS1.1 causes eRF1 degradation, together with RNF14 and RNF25.

Mammalian ISR can be activated by multiple kinases upon different stimuli.[47] Among those, the GCN1-GCN2 branch responds to translational disturbances such as amino acid starvation, UV treatment, and alkylating agents, which induce ribosome collisions.[49,50] Furthermore, robust ISR activation requires binding of GCN1 to ribosomes[51] and a cryo-EM structure revealed how GCN1 binds to stalled and collided disomes, suggesting that it acts as a collision sensor.[52] Considering GCN1's connection to ribosomal stalling and collisions, we hypothesized that NVS1.1 could directly influence translation termination and that eRF1 degradation might be a consequence of ribosome stalling at the stop codon. Supporting this hypothesis, incubating cells with the translation inhibitor cycloheximide rendered eRF1 immune to NVS1.1-mediated degradation (Figure 6B), revealing that NVS1.1 activity relies on active translation. Next, we investigated whether NVS1.1 alters the ribosome distribution on mRNAs by assessing polysome profiles from NVS1.1- and DMSO-treated cells. This revealed that NVS1.1 reduces the monosome peak and concomitantly increases the heavy polysome fraction (Figure 6C, left), potentially resulting from ribosome stalling accompanied by ribosome collisions. Under control conditions (DMSO), eRF1 is predominantly found in the light fractions of the gradient and hardly detectable in the polysome fractions. In contrast, NVS1.1 treatment caused a striking shift of partially ubiquitinated eRF1 into the heavy polysome fractions (Figure 6C, right), suggesting that NVS1.1 traps eRF1 on ribosomes and inhibits translation termination. By contrast, eRF3 did not co-migrate with ribosomes and remained in the light fractions when NVS1.1 was added. Considering that eRF1 and eRF3-GTP terminate translation as a ternary complex,[53] the absence of eRF3 in the polysome fractions of NVS1.1-treated cells indicates that translation termination can proceed until GTP hydrolysis and subsequent eRF3 dissociation but is blocked before eRF1 can leave the ribosome. We also assessed the distribution of EDF1, which binds to polysomes in a collision-dependent manner and recruits the translational repressors GIGYF2 and 4EHP to prevent new ribosomes from initiating translation on defective mRNAs.[54,55] In our experiments, EDF1 mainly resided in the light, ribosome-free fractions and in the monosome fraction under control conditions (DMSO). However, in NVS1.1-treated cells, a portion of EDF1 was detected in the polysome fractions (Figure 6C, right). Collectively, the accumulation of ubiquitinated eRF1 and EDF1 on polysomes suggests that NVS1.1 inhibits eRF1's function in translation termination, leading to ribosome stalling at stop codons and subsequent collisions with trailing ribosomes.

To further validate NVS1.1's effect on translation termination, we performed sucrose gradient fractionations of nuclease-digested lysates, which allows direct monitoring of ribosome collisions (Figure 6D, left).[49,55,56] Whereas, in control conditions (DMSO), polysomes collapsed upon digestion with Micrococcal nuclease (S7), treatment with low doses of Emetine, a well-established collision-inducing condition,[55,56] led to increased peaks for trisome and higher-order ribosome complexes (referred to as multisomes). NVS1.1 treatment led to similar multisome increase as emetine (Figure 6D, left). The analysis of individual fractions by immunoblot (Figure 6D, right) looked similar to that observed with the polysome gradients not treated with nuclease: NVS1.1 treatment shifted eRF1 to the multisome fractions (fraction 9 and higher) and only little eRF1 was present in the monosome fraction (fraction 7), indicating that trapped eRF1 is exclusively found in collided ribosomes. Interestingly, NVS1.1 did not change the distribution of GCN1. In the presence and absence of NVS1.1, most of the GCN1 protein was detected in the light fractions and decreasing amounts toward the heavy polysomes, indicating that GCN1 interacts with ribosomes even independently of collisions.

Ribosome collisions induce ubiquitination of ribosomal proteins, which serve as signals for a multi-layered downstream quality control process that mediates ribosome rescue and

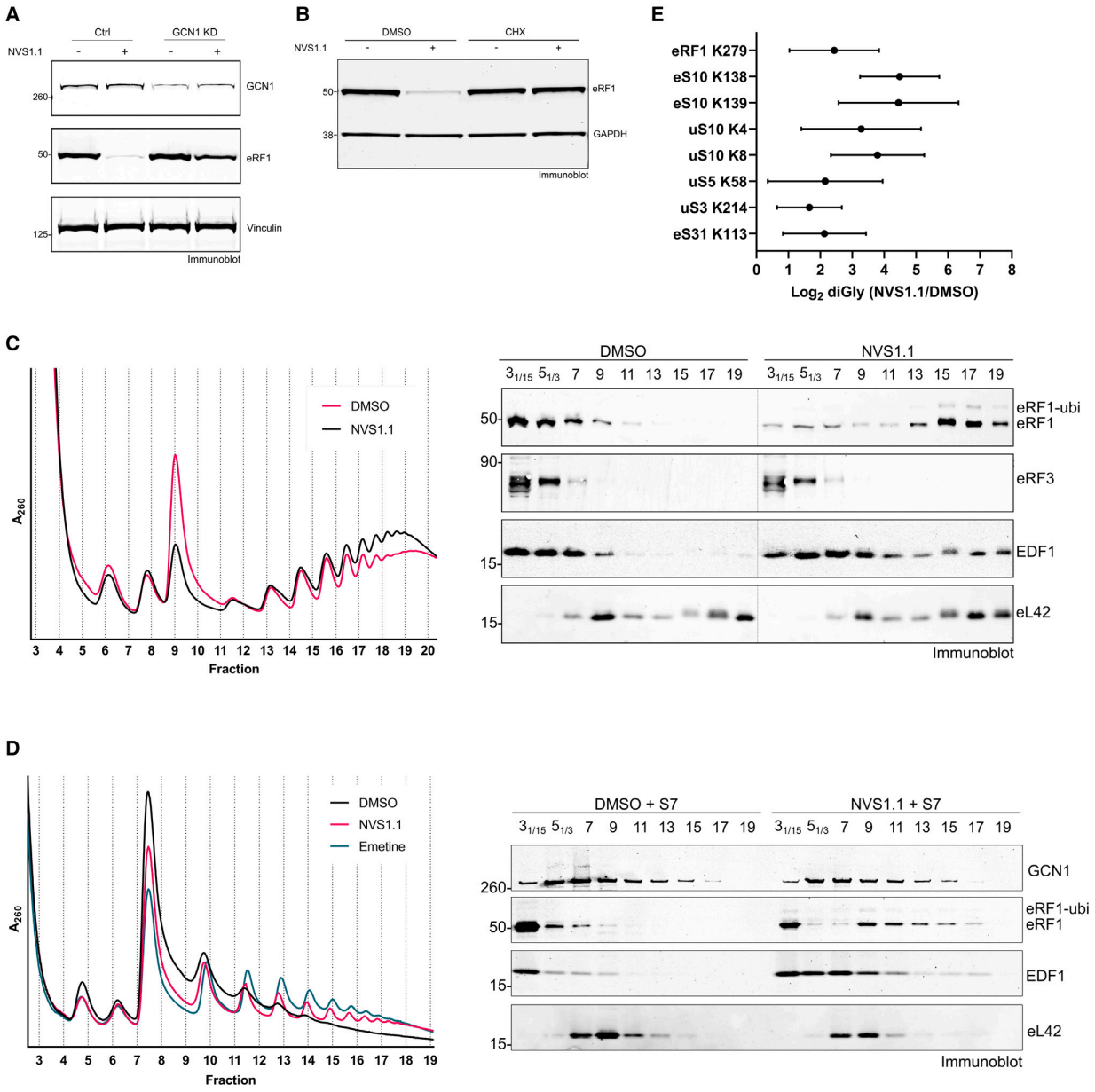


**Figure 6. NVS1.1 triggers GCN1-mediated RQC by trapping eRF1 on terminating ribosomes**

(A) Effects of GCN1 knockdown on eRF1 levels in HEKR4 cells treated with 2.5 μM NVS1.1 for 6 h. The immunoblot shows GCN1, eRF1, and vinculin (loading control) protein levels.

(B) Effects of cycloheximide (CHX) on eRF1 levels in HEKR4 cells treated with 2.5 μM NVS1.1 for 6 h. The immunoblot shows eRF1 and GAPDH (loading control) protein levels.

(C) Polysome profiling and protein analysis of fractions of HEKR4 cells treated with DMSO or 25 μM NVS1.1 for 30 min NVS1.1. Left panel: $A_{260}$ readout of cell lysate separated over a 15%–50% sucrose gradient. Right panel: proteins in odd-numbered fractions were precipitated and analyzed by immunoblotting for eRF1, eRF3, EDF1, and eL42 (RPL36a). Fractions 3 and 5 were diluted 1/15 and 1/3, respectively.

(D) Ribosome collision analysis in HEKR4 cells treated with 25 μM NVS1.1 for 30 min or 1.8 μM emetine for 15 min. Left panel: cells were lysed, digested, with Micrococcal nuclease S7, and then fractionated over a 15%–50% sucrose gradient as described in (C). Right panel: immunoblot analysis of odd-numbered gradient fractions for GCN1, eRF1, EDF1, and eL42.

(E) Ubiquitination analysis of eRF1 and ribosomal proteins in heavy polysome fractions (from C) treated with NVS1.1. Proteins were analyzed by mass spectrometry and diGly remnants on lysine residues were normalized to the corresponding protein abundance. The fold change of the diGly frequency ($log_2$ diGly [NVS1.1/DMSO]) is shown for eRF1 and for ribosomal proteins that showed a statistically significant difference ($p < 0.05$) upon NVS1.1 treatment.

recycling.[57] To assess whether NVS1.1 causes similar ubiquitin signatures, we analyzed heavy polysome fractions from Figure 6C by mass spectrometry. While the relative abundance of ribosomal proteins in polysomes was not affected by NVS1.1 (Table S4), multiple NVS1.1-specific ubiquitination events (detected as diGly remnants) on small subunit ribosomal proteins were detected, in addition to the eRF1 K279 ubiquitination (Figure 6E; Table S4). Most enriched were ubiquitination of eS10 (RPS10) on amino acids K138 and K139 and of uS10 (RPS20) on K4 and K8. eS10 and uS10 ubiquitination is mediated by the E3 ligase ZNF598, which recognizes the interface of collided ribosomes and thereby acts as a sentinel of translation by recognizing ribosome stalls and collisions.[56,58,59]

To test whether ZNF598 was also required for NVS1.1-mediated eRF1 degradation, we incubated ZNF598 KO HEK293 cells with NVS1.1 and observed unperturbed eRF1 depletion (Figure S6A). Thus, whereas eS10 and uS10 ubiquitination provides further evidence that NVS1.1 causes ribosome collisions, ZNF598 is not directly involved in the degradation of eRF1, consistent with the CRISPR screen results, in which ZNF598 was not a hit (Figures 5A and S5B). The detected ubiquitination of two other small subunit proteins, uS5 (RPS2) and uS3 (RPS3), was previously reported upon treatment of cells with various proteostasis stressors, including translation inhibitors and ISR agonists.[60] RNF10 was identified as the E3 ligase responsible for uS5 and uS3 ubiquitination and for regulating 40S subunit turnover in concert with the deubiquitinating enzyme USP10.[60,61] The signal for uS5 and uS3 ubiquitination appears to be distinct from ZNF598, hinting at translation initiation defects rather than elongation stalls, but the mechanistic details have yet to be revealed.[60,61] Finally, we detected increased eS31 (RPS27A) ubiquitination on K113. eS31 K107/K113 ubiquitination was previously observed upon treatment of cells with a low, ribosome collision-inducing concentration of Emetine.[55] Furthermore, loss of USP16—a deubiquitinase involved in 40S ribosomal subunit maturation—led to the accumulation of K113-ubiquitinated eS31 in a translation-dependent manner.[62] While the E3 ligase responsible for eS31 ubiquitination remained elusive, our data hint at RNF14 and/or RNF25.

In summary, our results reveal that NVS1.1 arrests translation by trapping eRF1 on terminating ribosomes, leading to eRF1 degradation by a pathway involving GCN1, RNF14, and RNF25. In parallel, the resulting ribosome collisions and translational repression trigger a series of ribosomal protein ubiquitination that involves different previously identified ribosome-associated quality control (RQC) mechanisms.

## DISCUSSION

We report here the development of new readthrough compounds with favorable pharmacokinetics and document their efficacy in cellular and animal disease models for CF and Hurler syndrome (Figures 1, 2, and 3). Unbiased high-throughput screening using cellular reporter models and compound triaging with multiple functional assays allowed the selection of promising small-molecular-weight compounds. Using patient-derived cells and animal tissues early in the assessment process increased the likelihood of identifying promising starting points for chemical optimization. Lead compounds were evaluated in Hurler patient-derived fibroblasts, aiding in the selection of promising scaffolds for optimization and *in vivo* tool compound characterization. The two most effective compounds, NVS1.1 and NVS2.1, are structurally diverse, have different pharmacokinetics and chemical properties but act mechanistically very similar (Figures 4–6). Different compounds with a similar mode of action are ideal to investigate their potential of promoting stop codon readthrough in multiple diseases. Early *in vivo* pharmacokinetic and pharmacodynamic assessments were performed in an engineered Hurler rat model that recapitulates the classical Hurler phenotype and biomarkers.[33] Upon NVS1.1 and NVS2.1 treatment, relatively modest amounts of restored full-length IDUA enzyme caused a pronounced and dose-dependent reduction of total GAG and of GUSB enzymatic activity in brain tissue. Further efficacy readouts such as reduction of enlarged lysosomal structures and inflammatory response reduction will be required to determine the clinical potential of the readthrough compounds. Furthermore, given that both compounds trigger eRF1 depletion, detailed safety assessments are crucial to determine their therapeutic potential.

Our investigation of NVS1.1's mode of action uncovered a GCN1-dependent mechanism that senses stalled ribosomes at stop codons upon NVS1.1 treatment. This activates a pathway involving the E3 ligases RNF14 and RNF25, which mark eRF1 for proteasomal degradation. Furthermore, we detect hallmarks of previously described RQC and stress response pathways, including ZNF598-mediated ubiquitination of ribosomal proteins, and NVS1.1-dependent EDF1 co-migration with polysomes, implying a multifaced cellular response pathway activated by NVS1.1-mediated inhibition of translation termination. The identification of GCN1, RNF14, and RNF25 as top hits in the CRISPR KO and siRNA screens performed with NVS2.1 (Figure S5B) suggests that both compounds, despite their different chemical scaffolds, inhibit translation termination by a common mechanism. This is further corroborated by another publication reporting that the compound SRI-41315 (Novartis patents WO2014/091446A1 and WO2015/186063A1), a derivative of NVS2, also causes eRF1 degradation in an RNF14- and RNF25-dependent manner.[63]

Interestingly, remarkably similar observations were reported for the cyclic peptide ternatin-4, an allosteric inhibitor of the elongation factor 1α (eEF1A).[63] Ternatin-4 induces the degradation of eEF1A by a pathway that also involves GCN1, RNF14, and RNF25. Paralleling our findings of NVS1.1-induced eRF1 ubiquitination and proteasomal decay, RNF14 and RNF25 were shown to promote eEF1A ubiquitination upon ternatin-4 treatment of cells. Combining the data of their study with our results, we propose the following model for the mode of action of NVS1.1 (Figure 7A): NVS1.1 traps eRF1 on terminating ribosomes, leading to collisions with trailing ribosomes. GCN1 senses these collisions and triggers ubiquitination of eRF1 in a process that requires the cooperative activity of the E3 ligases RNF14 and RNF25. Analogously to GCN1's interaction with GCN2, RNF14 and RNF25 both feature N-terminal RWD domains that could interact with GCN1's RWD binding domain (RWDBD).[64,65] Indeed, using reciprocal immunoprecipitations with overexpressed bait proteins, the binding of RNF14 (but not RNF25) with the RWDBD of GCN1 was confirmed.[63]

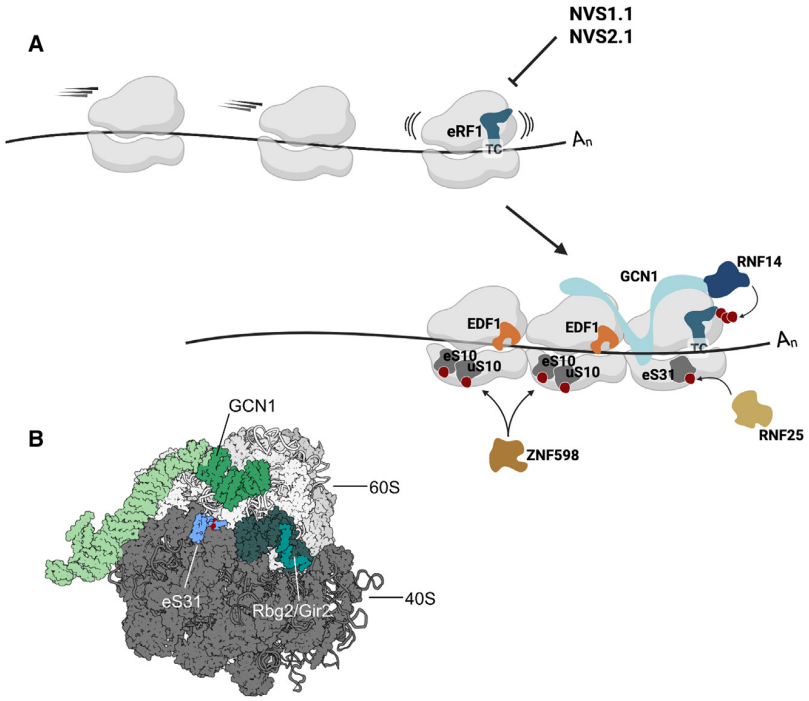


**Figure 7. Model for the NVS1.1 mode of action**

(A) Illustration of the GCN1-RNF14-RNF25-dependent translation quality control pathway that resolves ribosomal NVS compound-induced termination stalls by proteasomal degradation of eRF1. Red dots: ubiquitin. Created by BioRender.

(B) Cryo-EM structure of yeast GCN1-bound lead ribosome within a collided disome complex (PDB: 7NRC) showing the 40S (dark gray) and the 60S subunits (light gray). The GCN1 part is depicted in green, with its RWDBD domain in dark green. The GTPase Gir2 (teal) complexed with Rbg2 (dark teal) locates to the A site. eS31 (RPS27a) is depicted in blue, with K107 and K113 marked in red.

Noteworthy, the RNF14-GCN1 interaction occurred in the absence of ternatin-4.[63] Furthermore, our data indicate that GCN1 has a general affinity to ribosomes that is partly independent of ribosome collisions (Figure 6D), suggesting that formation of a ribosome-bound GCN1-RNF14 complex is not sufficient to activate the pathway but that an additional molecular cue is needed. To this end, we identified a set of ubiquitinated ribosomal proteins in response to the NVS1.1 treatment. Some are known markers for RQC events (uS5, uS3, eS10, and uS10), whereas the role of eS31 K113 ubiquitination is less well understood. Interestingly, ubiquitination of eS31 at K107 and K113 was also detected in ternatin-4-treated cells and depended on RNF25,[63] corroborating the notion that ubiquitination of ribosomal proteins is an integral part of the signaling leading to the degradation of eEF1A and eRF1. Notably, in the cryo-EM structure of GCN1 bound to two collided ribosomes, the RWDBD of GCN1 locates near the ubiquitination sites of eS31 on the small ribosomal subunit[52,63] (Figure 7B), suggesting that ubiquitinated eS31 could function as an allosteric activator of the GCN1-RNF14 complex. Collectively, our data indicate that NVS1.1-induced eRF1 ubiquitination by RNF14 requires multiple molecular inputs, including recognizing ribosome collisions by GCN1 and ubiquitination of ribosomal proteins—possibly mediated by RNF25 on eS31—as activating signal. Although further biochemical investigation is necessary to dissect the mechanistic details, our model provides a rationale for why two E3 ligases are required to degrade eRF1. Furthermore, this multistep activation might represent a mechanistic barrier preventing induction of eRF1 and eEF1A degradation during stochastically slow but functional termination and elongation events, respectively.

Despite similarities between the responses to ternatin-4[63] and NVS1.1, they target different proteins for degradation at distinct translation steps, raising the question of the underlying principle of these two processes. Ternatin-4 inhibits translation elongation by binding to the ternary complex consisting of aminoacyl-tRNA, eEF1A, and GTP and so perturbing tRNA accommodation. This traps eEF1A in the ribosomal A site and results in stalled ribosomes.[66] The binding site of NVS1.1 is currently unknown, yet our results indicate that it blocks translation termination by preventing eRF1 from leaving the ribosome. While both compounds target translational GTPase complexes, ternatin-4 targets the GTPase eEF1A for degradation, whereas NVS1.1 targets the decoding factor eRF1 and leaves the GTPase eRF3 unaffected. Therefore, we hypothesize that the degradation pathway involving GCN1, RNF14, and RNF25 recognizes and resolves generally stalled ribosomes with an occluded A site rather than recognizing specific proteins, which would be mechanistically distinct from previously described pathways that solve translational problems. For instance, the Pelota-Hbs1L complex preferentially acts on stalled ribosomes devoid of mRNA in the A site,[53,67] and structural data of collided ribosomes ubiquitinated by ZNF598 suggest that the primary recognition motif of ZNF598 is the contact of specific ribosomal proteins at the 40S-40S disome interface, independent of the A site occupancy.[56,43] Collectively, we postulate that GCN1, RNF14, and RNF25 comprise a branch of RQC that resolves ribosome problems arising from an occluded A site during translation elongation and termination.

GCN1 was so far best known for its role in GCN2-dependent activation of the ISR upon sensing ribosome collisions.[49,50] Our findings suggest that GCN1 serves as a broader sensor of ribosome stalling, leading to the activation of distinct downstream pathways depending on the cause of the stalling. Whereas empty A sites reduce translation initiation via ISR activation, occluded A sites trigger proteasomal degradation of the obstructing protein. In the NVS1.1-mediated inhibition of translation termination, the A site obstructor is eRF1 and its rapid RNF14-RNF25-proteasome-mediated depletion results in increased readthrough of TCs, explaining why NVS1.1 is a potent readthrough promoter. Additional work is needed to elucidate the links between GCN1- and ZNF598-mediated responses to ribosome stalls and the conditions that trigger these pathways. Furthermore, it remains to be

investigated how ribosomal subunits are recycled after eRF1 ubiquitination and at which stage eRF1 is subjected to proteasomal degradation. Apart from their therapeutic potential, the compounds NVS1.1 and NVS2.1 will provide useful tools to further dissect the intricate network of RQC mechanisms.

### Limitations of the study

While our study demonstrated how the small-molecule compounds NVS1.1 and NVS2.1 lead to ribosome stalling at a PTC and to the GCN1-mediated activation of RQC, it remains to be elucidated under which physiological conditions occluded A sites occur that trigger this pathway. However, the finding that overexpression of Itt1p, the RNF14 homolog in *S. cerevisiae*, also causes eRF1 depletion[68] suggests an evolutionary conservation and physiological functions of this GCN1-RNF14-RNF25-dependent translation quality control. To evaluate the clinical potential of NVS2.1, NVS1.1, and their derivates extensive combined pharmacology and toxicology studies are needed and a detailed safety assessment and risk/benefit analysis is mandatory.

## STAR★METHODS

Detailed methods are provided in the online version of this paper and include the following:

- KEY RESOURCES TABLE
- RESOURCE AVAILABILITY
  - Lead contact
  - Materials availability
  - Data and code availability
- EXPERIMENTAL MODEL AND STUDY PARTICIPANT DETAILS
  - Cell lines and culture conditions
  - Engineering of recombinant PTC reporter, CFTR and IDUA cell models
  - Engineering of knockout and rescue cell lines
  - Hurler IDUA-W401X rat model engineering and compound administration
- METHOD DETAILS
  - siRNA-mediated knockdown of GCN1
  - High throughput screening and hit filtering
  - siRNA screen
  - CRISPR screening procedures
  - Cell line sensitivity to NVS1.1 and NVS2.1
  - Library transduction
  - Preparation of genomic DNA
  - Illumina flowcell generation and sequencing
  - CRISPR screening
  - Hit analysis
  - CFTR expression assessment by immunofluorescence microscopy
  - CFTR membrane potential assay
  - RT-qPCR in Hurler patient-derived fibroblasts
  - Rat *in vitro and in vivo* studies
  - Brain tissue analysis
  - Determination of the NVS1.1 and NVS2.1 concentration in the CSF
  - IDUA and GUSB enzyme assay
  - Total GAG assay
  - Immunoblot
  - Immunoprecipitation
  - Polysome fractionation
  - SILAC experiment in HEK293T cells to assess whole proteome changes under NVS1.1 treatment
  - Determination of amino acid inserted at stop codon
  - NanoLC-MS/MS - Parallel reaction monitoring (PRM)
  - Label-free mass spectrometry for whole proteome and ubiquitination analysis
- QUANTIFICATION AND STATISTICAL ANALYSIS

## SUPPLEMENTAL INFORMATION

Supplemental information can be found online at https://doi.org/10.1016/j.celrep.2023.113056.

## ACKNOWLEDGMENTS

The authors are grateful to Jane Nagel at NIBR Cambridge and Sophie Braga Lagache, Natasha Buchs, and Manfred Heller from the PMSCF of the University of Bern for their excellent mass spectrometry services; the former team and Novartis colleagues Lloyd Klickstein, Ken Huttner, Natalie Dales, Florian Fuchs, and Joseph Kelleher for translational medicine chemistry, and MoA work; Steffi Harlfinger for guiding the PK/PD *in vivo* work; Nicole Renaud and Jia Wu for NIBR data science support; Daniel Boehringer from the cryo-EM Hub of the ETH Zürich for help in comparing structural models; and Evangelos Karousis and Sofia Nasif from the Mühlemann lab for their valuable comments on the manuscript. We further acknowledge the ChemG and target ID proteomic groups at Novartis Cambridge, USA and Basel, CH and the Novartis CBT and DAx management for supporting the project. The work conducted at the University of Bern was supported by the National Center of Competence in Research (NCCR) on RNA & Disease funded by the Swiss National Science Foundation (SNSF) (grants 51NF40-141735, 182880, and 205601), by SNSF grants (310030B-182831 and 310030-204161), and by the Canton of Bern (University intramural funding to O.M.).

## AUTHOR CONTRIBUTIONS

J.R. and N.S. led the project and supervised and coordinated both the drug discovery *in vitro* and *in vivo* and the Novartis mode-of-action (MoA) work. I.S., Y.I., and O.G. conducted the HTS screens. N.S. chemically optimized the compounds. J.S. and C.G.-D. supported cell biology work. C.N.P. and I.S. did the CRISPR screen. X.M. supported the *in vivo* and rat cell work. F.B. was responsible for MS analysis. P.C. guided safety-related work. F.S. and M.S. guided the siRNA, SILAC, and MoA proteomic experiments. O.M. supervised the Bern MoA studies. L.-A.G. performed and analyzed the MoA experiments with contributions from J.Z. and W.T. A.-C.U. analyzed the proteomics data. L.-A.G. prepared all figures. L.-A.G., O.M., and J.R. wrote the manuscript.

## DECLARATION OF INTERESTS

L.-A.G., J.Z., A.-C.U., W.T., and O.M. declare no conflict of interest. N.S. and J.R. are authors on the related Novartis patents WO 2014/091446 A1 and WO 2015/186063 A1. Novartis claims interest according to these patents. N.S. and J.R. are employees and shareholders of Novartis Pharma AG.

Received: February 14, 2023
Revised: June 15, 2023
Accepted: August 16, 2023

## REFERENCES


1. Mort, M., Ivanov, D., Cooper, D.N., and Chuzhanova, N.A. (2008). A meta-analysis of nonsense mutations causing human genetic disease. Hum. Mutat. *29*, 1037–1047. https://doi.org/10.1002/humu.20763.
2. Brooks, D.A., Muller, V.J., and Hopwood, J.J. (2006). Stop-codon read-through for patients affected by a lysosomal storage disorder. Trends Mol. Med. *12*, 367–373. https://doi.org/10.1016/j.molmed.2006.06.001.
3. Dabrowski, M., Bukowy-Bieryllo, Z., and Zietkiewicz, E. (2018). Advances in therapeutic use of a drug-stimulated translational readthrough of premature termination codons. Mol. Med. *24*, 25. https://doi.org/10.1186/s10020-018-0024-7.
4. Lee, H.L.R., and Dougherty, J.P. (2012). Pharmaceutical therapies to recode nonsense mutations in inherited diseases. Pharmacol. Ther. *136*, 227–266. https://doi.org/10.1016/j.pharmthera.2012.07.007.
5. Nagel-Wolfrum, K., Möller, F., Penner, I., Baasov, T., and Wolfrum, U. (2016). Targeting Nonsense Mutations in Diseases with Translational Read-Through-Inducing Drugs (TRIDs). BioDrugs *30*, 49–74. https://doi.org/10.1007/s40259-016-0157-6.
6. Sabbavarapu, N.M., Shavit, M., Degani, Y., Smolkin, B., Belakhov, V., and Baasov, T. (2016). Design of Novel Aminoglycoside Derivatives with Enhanced Suppression of Diseases-Causing Nonsense Mutations. ACS Med. Chem. Lett. *7*, 418–423. https://doi.org/10.1021/acsmedchemlett.6b00006.
7. Guan, M.X., Fischel-Ghodsian, N., and Attardi, G. (2000). A biochemical basis for the inherited susceptibility to aminoglycoside ototoxicity. Hum. Mol. Genet. *9*, 1787–1793. https://doi.org/10.1093/hmg/9.12.1787.
8. Welch, E.M., Barton, E.R., Zhuo, J., Tomizawa, Y., Friesen, W.J., Trifillis, P., Paushkin, S., Patel, M., Trotta, C.R., Hwang, S., et al. (2007). PTC124 targets genetic disorders caused by nonsense mutations. Nature *447*, 87–91.
9. Gonzalez-Hilarion, S., Beghyn, T., Jia, J., Debreuck, N., Berte, G., Mamchaoui, K., Mouly, V., Gruenert, D.C., Déprez, B., and Lejeune, F. (2012). Rescue of nonsense mutations by amlexanox in human cells. Orphanet J. Rare Dis. *7*, 58. https://doi.org/10.1186/1750-1172-7-58.
10. Alkalaeva, E.Z., Pisarev, A.V., Frolova, L.Y., Kisselev, L.L., and Pestova, T.V. (2006). In vitro reconstitution of eukaryotic translation reveals cooperativity between release factors eRF1 and eRF3. Cell *125*, 1125–1136. https://doi.org/10.1016/j.cell.2006.04.035.
11. Frolova, L., Le Goff, X., Rasmussen, H.H., Cheperegin, S., Drugeon, G., Kress, M., Arman, I., Haenni, A.L., Celis, J.E., Philippe, M., et al. (1994). A highly conserved eukaryotic protein family possessing properties of polypeptide chain release factor. Nature *372*, 701–703. https://doi.org/10.1038/372701a0.
12. Zhouravleva, G., Frolova, L., Le Goff, X., Le Guellec, R., Inge-Vechtomov, S., Kisselev, L., and Philippe, M. (1995). Termination of translation in eukaryotes is governed by two interacting polypeptide chain release factors, eRF1 and eRF3. EMBO J. *14*, 4065–4072. https://doi.org/10.1002/j.1460-2075.1995.tb00078.x.
13. Lawson, M.R., Lessen, L.N., Wang, J., Prabhakar, A., Corsepius, N.C., Green, R., and Puglisi, J.D. (2021). Mechanisms that ensure speed and fidelity in eukaryotic translation termination. Science *373*, 876–882. https://doi.org/10.1126/science.abi7801.
14. Wangen, J.R., and Green, R. (2020). Stop codon context influences genome-wide stimulation of termination codon readthrough by aminoglycosides. Elife *9*, e52611. https://doi.org/10.7554/eLife.52611.
15. Manuvakhova, M., Keeling, K., and Bedwell, D.M. (2000). Aminoglycoside antibiotics mediate context-dependent suppression of termination codons in a mammalian translation system. RNA *6*, 1044–1055.
16. Keeling, K.M., Xue, X., Gunn, G., and Bedwell, D.M. (2014). Therapeutics based on stop codon readthrough. Annu. Rev. Genom. Hum. Genet. *15*, 371–394. https://doi.org/10.1146/annurev-genom-091212-153527.
17. Biziaev, N., Sokolova, E., Yanvarev, D.V., Toropygin, I.Y., Shuvalov, A., Egorova, T., and Alkalaeva, E. (2022). Recognition of 3' nucleotide context and stop codon readthrough are determined during mRNA translation elongation. J. Biol. Chem. *298*, 102133. https://doi.org/10.1016/j.jbc.2022.102133.
18. Howard, M., DuVall, M.D., Devor, D.C., Dong, J.Y., Henze, K., and Frizzell, R.A. (1995). Epitope tagging permits cell surface detection of functional CFTR. Am. J. Physiol. *269*, C1565–C1576. https://doi.org/10.1152/ajpcell.1995.269.6.C1565.
19. Liu, M., Liao, H., Chen, Y., Lin, Z., Liu, Y., Zhang, X., Chan, H.C., and Sun, H. (2019). Treatment of human T-cell acute lymphoblastic leukemia cells with CFTR inhibitor CFTRinh-172. Leuk. Res. *86*, 106225. https://doi.org/10.1016/j.leukres.2019.106225.
20. Roy, B., Leszyk, J.D., Mangus, D.A., and Jacobson, A. (2015). Nonsense suppression by near-cognate tRNAs employs alternative base pairing at codon positions 1 and 3. Proc. Natl. Acad. Sci. USA *112*, 3038–3043. https://doi.org/10.1073/pnas.1424127112.
21. Ong, S.E., Blagoev, B., Kratchmarova, I., Kristensen, D.B., Steen, H., Pandey, A., and Mann, M. (2002). Stable isotope labeling by amino acids in cell culture, SILAC, as a simple and accurate approach to expression proteomics. Mol. Cell. Proteomics *1*, 376–386. https://doi.org/10.1074/mcp.m200025-mcp200.
22. Baradaran-Heravi, A., Balgi, A.D., Hosseini-Farahabadi, S., Choi, K., Has, C., and Roberge, M. (2021). Effect of small molecule eRF3 degraders on premature termination codon readthrough. Nucleic Acids Res. *49*, 3692–3708. https://doi.org/10.1093/nar/gkab194.
23. Carnes, J., Jacobson, M., Leinwand, L., and Yarus, M. (2003). Stop codon suppression via inhibition of eRF1 expression. RNA *9*, 648–653. https://doi.org/10.1261/rna.5280103.
24. Janzen, D.M., and Geballe, A.P. (2004). The effect of eukaryotic release factor depletion on translation termination in human cell lines. Nucleic Acids Res. *32*, 4491–4502. https://doi.org/10.1093/nar/gkh791.
25. Chauvin, C., and Jean-Jean, O. (2008). Proteasomal degradation of human release factor eRF3a regulates translation termination complex formation. RNA *14*, 240–245. https://doi.org/10.1261/rna.728608.
26. Sharma, J., Du, M., Wong, E., Mutyam, V., Li, Y., Chen, J., Wangen, J., Thrasher, K., Fu, L., Peng, N., et al. (2021). A small molecule that induces translational readthrough of CFTR nonsense mutations by eRF1 depletion. Nat. Commun. *12*, 4358. https://doi.org/10.1038/s41467-021-24575-x.
27. Beck, M., Arn, P., Giugliani, R., Muenzer, J., Okuyama, T., Taylor, J., and Fallet, S. (2014). The natural history of MPS I: global perspectives from the MPS I Registry. Genet. Med. *16*, 759–765. https://doi.org/10.1038/gim.2014.25.
28. Hein, L.K., Bawden, M., Muller, V.J., Sillence, D., Hopwood, J.J., and Brooks, D.A. (2004). alpha-L-iduronidase premature stop codons and potential read-through in mucopolysaccharidosis type I patients. J. Mol. Biol. *338*, 453–462. https://doi.org/10.1016/j.jmb.2004.03.012.
29. Keeling, K.M., Brooks, D.A., Hopwood, J.J., Li, P., Thompson, J.N., and Bedwell, D.M. (2001). Gentamicin-mediated suppression of Hurler syndrome stop mutations restores a low level of alpha-L-iduronidase activity and reduces lysosomal glycosaminoglycan accumulation. Hum. Mol. Genet. *10*, 291–299. https://doi.org/10.1093/hmg/10.3.291.
30. Ashton, L.J., Brooks, D.A., McCourt, P.A., Muller, V.J., Clements, P.R., and Hopwood, J.J. (1992). Immunoquantification and enzyme kinetics of alpha-L-iduronidase in cultured fibroblasts from normal controls and mucopolysaccharidosis type I patients. Am. J. Hum. Genet. *50*, 787–794.
31. Bunge, S., Clements, P.R., Byers, S., Kleijer, W.J., Brooks, D.A., and Hopwood, J.J. (1998). Genotype-phenotype correlations in mucopolysaccharidosis type I using enzyme kinetics, immunoquantification and in vitro turnover studies. Biochim. Biophys. Acta *1407*, 249–256. https://doi.org/10.1016/s0925-4439(98)00046-5.
32. Gunn, G., Dai, Y., Du, M., Belakhov, V., Kandasamy, J., Schoeb, T.R., Baasov, T., Bedwell, D.M., and Keeling, K.M. (2014). Long-term nonsense

suppression therapy moderates MPS I-H disease progression. Mol. Genet. Metabol. *111*, 374–381. https://doi.org/10.1016/j.ymgme.2013.12.007.

33. Wang, D., Shukla, C., Liu, X., Schoeb, T.R., Clarke, L.A., Bedwell, D.M., and Keeling, K.M. (2010). Characterization of an MPS I-H knock-in mouse that carries a nonsense mutation analogous to the human IDUA-W402X mutation. Mol. Genet. Metabol. *99*, 62–71. https://doi.org/10.1016/j.ymgme.2009.08.002.
34. Hogg, J.R., and Goff, S.P. (2010). Upf1 senses 3'UTR length to potentiate mRNA decay. Cell *143*, 379–389. https://doi.org/10.1016/j.cell.2010.10.005.
35. Bezstarosti, K., van der Wal, L., and Demmers, J.A.A. (2020). Detection of Protein Ubiquitination Sites by Peptide Enrichment and Mass Spectrometry. J. Vis. Exp. https://doi.org/10.3791/59079.
36. Matyskiela, M.E., Lu, G., Ito, T., Pagarigan, B., Lu, C.C., Miller, K., Fang, W., Wang, N.Y., Nguyen, D., Houston, J., et al. (2016). A novel cereblon modulator recruits GSPT1 to the CRL4(CRBN) ubiquitin ligase. Nature *535*, 252–257. https://doi.org/10.1038/nature18611.
37. Surka, C., Jin, L., Mbong, N., Lu, C.C., Jang, I.S., Rychak, E., Mendy, D., Clayton, T., Tindall, E., Hsu, C., et al. (2021). CC-90009, a novel cereblon E3 ligase modulator, targets acute myeloid leukemia blasts and leukemia stem cells. Blood *137*, 661–677. https://doi.org/10.1182/blood.2020008676.
38. Zhao, M., Hu, M., Chen, Y., Liu, H., Chen, Y., Liu, B., and Fang, B. (2021). Cereblon modulator CC-885 induces CRBN-dependent ubiquitination and degradation of CDK4 in multiple myeloma. Biochem. Biophys. Res. Commun. *549*, 150–156. https://doi.org/10.1016/j.bbrc.2021.02.110.
39. Ohmura-Hoshino, M., Goto, E., Matsuki, Y., Aoki, M., Mito, M., Uematsu, M., Hotta, H., and Ishido, S. (2006). A novel family of membrane-bound E3 ubiquitin ligases. J. Biochem. *140*, 147–154. https://doi.org/10.1093/jb/mvj160.
40. Kikuchi, H., Uchida, C., Hattori, T., Isobe, T., Hiramatsu, Y., Kitagawa, K., Oda, T., Konno, H., and Kitagawa, M. (2007). ARA54 is involved in transcriptional regulation of the cyclin D1 gene in human cancer cells. Carcinogenesis *28*, 1752–1758. https://doi.org/10.1093/carcin/bgm120.
41. Wu, B., Piloto, S., Zeng, W., Hoverter, N.P., Schilling, T.F., and Waterman, M.L. (2013). Ring Finger Protein 14 is a new regulator of TCF/beta-catenin-mediated transcription and colon cancer cell survival. EMBO Rep. *14*, 347–355. https://doi.org/10.1038/embor.2013.19.
42. Asamitsu, K., Tetsuka, T., Kanazawa, S., and Okamoto, T. (2003). RING finger protein AO7 supports NF-kappaB-mediated transcription by interacting with the transactivation domain of the p65 subunit. J. Biol. Chem. *278*, 26879–26887. https://doi.org/10.1074/jbc.M211831200.
43. Ikeuchi, K., Tesina, P., Matsuo, Y., Sugiyama, T., Cheng, J., Saeki, Y., Tanaka, K., Becker, T., Beckmann, R., and Inada, T. (2019). Collided ribosomes form a unique structural interface to induce Hel2-driven quality control pathways. EMBO J. *38*, e100276. https://doi.org/10.15252/embj.2018100276.
44. Ito, K., Adachi, S., Iwakami, R., Yasuda, H., Muto, Y., Seki, N., and Okano, Y. (2001). N-Terminally extended human ubiquitin-conjugating enzymes (E2s) mediate the ubiquitination of RING-finger proteins, ARA54 and RNF8. Eur. J. Biochem. *268*, 2725–2732. https://doi.org/10.1046/j.1432-1327.2001.02169.x.
45. Lorick, K.L., Jensen, J.P., Fang, S., Ong, A.M., Hatakeyama, S., and Weissman, A.M. (1999). RING fingers mediate ubiquitin-conjugating enzyme (E2)-dependent ubiquitination. Proc. Natl. Acad. Sci. USA *96*, 11364–11369. https://doi.org/10.1073/pnas.96.20.11364.
46. Costa-Mattioli, M., and Walter, P. (2020). The integrated stress response: From mechanism to disease. Science *368*, eaat5314. https://doi.org/10.1126/science.aat5314.
47. Pakos-Zebrucka, K., Koryga, I., Mnich, K., Ljujic, M., Samali, A., and Gorman, A.M. (2016). The integrated stress response. EMBO Rep. *17*, 1374–1395. https://doi.org/10.15252/embr.201642195.
48. Marton, M.J., Vazquez de Aldana, C.R., Qiu, H., Chakraburtty, K., and Hinnebusch, A.G. (1997). Evidence that GCN1 and GCN20, translational regulators of GCN4, function on elongating ribosomes in activation of eIF2alpha kinase GCN2. Mol. Cell Biol. *17*, 4474–4489. https://doi.org/10.1128/MCB.17.8.4474.
49. Wu, C.C.C., Peterson, A., Zinshteyn, B., Regot, S., and Green, R. (2020). Ribosome Collisions Trigger General Stress Responses to Regulate Cell Fate. Cell *182*, 404–416.e14. https://doi.org/10.1016/j.cell.2020.06.006.
50. Yan, L.L., and Zaher, H.S. (2021). Ribosome quality control antagonizes the activation of the integrated stress response on colliding ribosomes. Mol. Cell *81*, 614–628.e4. https://doi.org/10.1016/j.molcel.2020.11.033.
51. Sattlegger, E., and Hinnebusch, A.G. (2005). Polyribosome binding by GCN1 is required for full activation of eukaryotic translation initiation factor 2alpha kinase GCN2 during amino acid starvation. J. Biol. Chem. *280*, 16514–16521. https://doi.org/10.1074/jbc.M414566200.
52. Pochopien, A.A., Beckert, B., Kasvandik, S., Berninghausen, O., Beckmann, R., Tenson, T., and Wilson, D.N. (2021). Structure of Gcn1 bound to stalled and colliding 80S ribosomes. Proc. Natl. Acad. Sci. USA *118*, e2022756118. https://doi.org/10.1073/pnas.2022756118.
53. Shao, S., Murray, J., Brown, A., Taunton, J., Ramakrishnan, V., and Hegde, R.S. (2016). Decoding Mammalian Ribosome-mRNA States by Translational GTPase Complexes. Cell *167*, 1229–1240.e15. https://doi.org/10.1016/j.cell.2016.10.046.
54. Juszkiewicz, S., Slodkowicz, G., Lin, Z., Freire-Pritchett, P., Peak-Chew, S.Y., and Hegde, R.S. (2020). Ribosome collisions trigger cis-acting feedback inhibition of translation initiation. Elife *9*, e60038. https://doi.org/10.7554/eLife.60038.
55. Sinha, N.K., Ordureau, A., Best, K., Saba, J.A., Zinshteyn, B., Sundaramoorthy, E., Fulzele, A., Garshott, D.M., Denk, T., Thoms, M., et al. (2020). EDF1 coordinates cellular responses to ribosome collisions. Elife *9*, e58828. https://doi.org/10.7554/eLife.58828.
56. Juszkiewicz, S., Chandrasekaran, V., Lin, Z., Kraatz, S., Ramakrishnan, V., and Hegde, R.S. (2018). ZNF598 Is a Quality Control Sensor of Collided Ribosomes. Mol. Cell *72*, 469–481.e7. https://doi.org/10.1016/j.molcel.2018.08.037.
57. Kim, K.Q., and Zaher, H.S. (2022). Canary in a coal mine: collided ribosomes as sensors of cellular conditions. Trends Biochem. Sci. *47*, 82–97. https://doi.org/10.1016/j.tibs.2021.09.001.
58. Garzia, A., Jafarnejad, S.M., Meyer, C., Chapat, C., Gogakos, T., Morozov, P., Amiri, M., Shapiro, M., Molina, H., Tuschl, T., and Sonenberg, N. (2017). The E3 ubiquitin ligase and RNA-binding protein ZNF598 orchestrates ribosome quality control of premature polyadenylated mRNAs. Nat. Commun. *8*, 16056. https://doi.org/10.1038/ncomms16056.
59. Sundaramoorthy, E., Leonard, M., Mak, R., Liao, J., Fulzele, A., and Bennett, E.J. (2017). ZNF598 and RACK1 Regulate Mammalian Ribosome-Associated Quality Control Function by Mediating Regulatory 40S Ribosomal Ubiquitylation. Mol. Cell *65*, 751–760.e4. https://doi.org/10.1016/j.molcel.2016.12.026.
60. Higgins, R., Gendron, J.M., Rising, L., Mak, R., Webb, K., Kaiser, S.E., Zuzow, N., Riviere, P., Yang, B., Fenech, E., et al. (2015). The Unfolded Protein Response Triggers Site-Specific Regulatory Ubiquitylation of 40S Ribosomal Proteins. Mol. Cell *59*, 35–49. https://doi.org/10.1016/j.molcel.2015.04.026.
61. Garzia, A., Meyer, C., and Tuschl, T. (2021). The E3 ubiquitin ligase RNF10 modifies 40S ribosomal subunits of ribosomes compromised in translation. Cell Rep. *36*, 109468. https://doi.org/10.1016/j.celrep.2021.109468.
62. Montellese, C., van den Heuvel, J., Ashiono, C., Dörner, K., Melnik, A., Jonas, S., Zemp, I., Picotti, P., Gillet, L.C., and Kutay, U. (2020). USP16 counteracts mono-ubiquitination of RPS27a and promotes maturation of the 40S ribosomal subunit. Elife *9*, e54435. https://doi.org/10.7554/eLife.54435.
63. Oltion, K., Carelli, J.D., Yang, T., See, S.K., Wang, H.Y., Kampmann, M., and Taunton, J. (2023). An E3 ligase network engages GCN1 to promote the degradation of translation factors on stalled ribosomes. Cell *186*, 346–362.e17. https://doi.org/10.1016/j.cell.2022.12.025.
64. Kubota, H., Sakaki, Y., and Ito, T. (2000). GI domain-mediated association of the eukaryotic initiation factor 2alpha kinase GCN2 with its activator

GCN1 is required for general amino acid control in budding yeast. J. Biol. Chem. *275*, 20243–20246. https://doi.org/10.1074/jbc.C000262200.

65. Sattlegger, E., and Hinnebusch, A.G. (2000). Separate domains in GCN1 for binding protein kinase GCN2 and ribosomes are required for GCN2 activation in amino acid-starved cells. EMBO J. *19*, 6622–6633. https://doi.org/10.1093/emboj/19.23.6622.

66. Juette, M.F., Carelli, J.D., Rundlet, E.J., Brown, A., Shao, S., Ferguson, A., Wasserman, M.R., Holm, M., Taunton, J., and Blanchard, S.C. (2022). Didemnin B and ternatin-4 differentially inhibit conformational changes in eEF1A required for aminoacyl-tRNA accommodation into mammalian ribosomes. Elife *11*, e81608. https://doi.org/10.7554/eLife.81608.

67. Hilal, T., Yamamoto, H., Loerke, J., Bürger, J., Mielke, T., and Spahn, C.M.T. (2016). Structural insights into ribosomal rescue by Dom34 and Hbs1 at near-atomic resolution. Nat. Commun. *7*, 13521. https://doi.org/10.1038/ncomms13521.

68. Urakov, V.N., Valouev, I.A., Lewitin, E.I., Paushkin, S.V., Kosorukov, V.S., Kushnirov, V.V., Smirnov, V.N., and Ter-Avanesyan, M.D. (2001). Itt1p, a novel protein inhibiting translation termination in Saccharomyces cerevisiae. BMC Mol. Biol. *2*, 9. https://doi.org/10.1186/1471-2199-2-9.

69. Zhang, J.H., Chung, T.D., and Oldenburg, K.R. (1999). A Simple Statistical Parameter for Use in Evaluation and Validation of High Throughput Screening Assays. J. Biomol. Screen *4*, 67–73. https://doi.org/10.1177/108705719900400206.

70. König, R., Chiang, C.Y., Tu, B.P., Yan, S.F., DeJesus, P.D., Romero, A., Bergauer, T., Orth, A., Krueger, U., Zhou, Y., and Chanda, S.K. (2007). A probability-based approach for the analysis of large-scale RNAi screens. Nat. Methods *4*, 847–849. https://doi.org/10.1038/nmeth1089.

71. Schmittgen, T.D., and Livak, K.J. (2008). Analyzing real-time PCR data by the comparative C(T) method. Nat. Protoc. *3*, 1101–1108. https://doi.org/10.1038/nprot.2008.73.

72. Pegg, C.C., He, C., Stroink, A.R., Kattner, K.A., and Wang, C.X. (2010). Technique for collection of cerebrospinal fluid from the cisterna magna in rat. J. Neurosci. Methods *187*, 8–12. https://doi.org/10.1016/j.jneumeth.2009.12.002.

73. Shevchenko, A., Tomas, H., Havlis, J., Olsen, J.V., and Mann, M. (2006). In-gel digestion for mass spectrometric characterization of proteins and proteomes. Nat. Protoc. *1*, 2856–2860. https://doi.org/10.1038/nprot.2006.468.

74. Peterson, A.C., Russell, J.D., Bailey, D.J., Westphall, M.S., and Coon, J.J. (2012). Parallel reaction monitoring for high resolution and high mass accuracy quantitative, targeted proteomics. Mol. Cell. Proteomics *11*, 1475–1488. https://doi.org/10.1074/mcp.O112.020131.

75. da Veiga Leprevost, F., Haynes, S.E., Avtonomov, D.M., Chang, H.Y., Shanmugam, A.K., Mellacheruvu, D., Kong, A.T., and Nesvizhskii, A.I. (2020). Philosopher: a versatile toolkit for shotgun proteomics data analysis. Nat. Methods *17*, 869–870. https://doi.org/10.1038/s41592-020-0912-y.

76. Kong, A.T., Leprevost, F.V., Avtonomov, D.M., Mellacheruvu, D., and Nesvizhskii, A.I. (2017). MSFragger: ultrafast and comprehensive peptide identification in mass spectrometry-based proteomics. Nat. Methods *14*, 513–520. https://doi.org/10.1038/nmeth.4256.

77. Yu, F., Haynes, S.E., and Nesvizhskii, A.I. (2021). IonQuant Enables Accurate and Sensitive Label-Free Quantification With FDR-Controlled Match-Between-Runs. Mol. Cell. Proteomics *20*, 100077. https://doi.org/10.1016/j.mcpro.2021.100077.

78. UniProt Consortium (2019). UniProt: a worldwide hub of protein knowledge. Nucleic Acids Res. *47*, D506–D515. https://doi.org/10.1093/nar/gky1049.

79. Silver, J.D., Ritchie, M.E., and Smyth, G.K. (2009). Microarray background correction: maximum likelihood estimation for the normal-exponential convolution. Biostatistics *10*, 352–363. https://doi.org/10.1093/biostatistics/kxn042.

80. Uldry, A.C., Maciel-Dominguez, A., Jornod, M., Buchs, N., Braga-Lagache, S., Brodard, J., Jankovic, J., Bonadies, N., and Heller, M. (2022). Effect of Sample Transportation on the Proteome of Human Circulating Blood Extracellular Vesicles. Int. J. Mol. Sci. *23*, 4515. https://doi.org/10.3390/ijms23094515.

## STAR★METHODS

### KEY RESOURCES TABLE

| REAGENT or RESOURCE | SOURCE | IDENTIFIER |
|---|---|---|
| **Antibodies** | | |
| anti-eRF1, rabbit (immunoblot, 1:3′000) | Abcam | Cat# ab31799; RRID:AB_732264 |
| anti-eRF1, mouse (IP) | Santa Cruz Biotechnology | Cat# sc-365686; RRID:AB_10843214 |
| anti-GAPDH, mouse (1:2′000) | Santa Cruz Biotechnology | Cat# sc-47724; RRID:AB_627678 |
| anti-ubiquitin, mouse (1:100) | Santa Cruz Biotechnology | Cat# sc-271289; RRID:AB_10611436 |
| anti-vinculin, mouse (1:1′000) | Santa Cruz Biotechnology | Cat# sc-73614; RRID:AB_1131294 |
| anti-RNF14, rabbit (1:1′000) | Sigma-Aldrich | Cat# HPA008716; RRID:AB_1856337 |
| anti-EDF1, rabbit (1:2′000) | Abcam | Cat# ab174651; RRID:AB_2893192 |
| anti-eRF3 (1:1′000) | Abcam | Cat# ab49878; RRID:AB_2115507 |
| anti-RNF25, rabbit (1:1′000) | Bethyl Laboratories | Cat# A303-844A; RRID:AB_2620195 |
| anti-GCN1, rabbit (1:2′000) | Bethyl Laboratories | Cat# A301-843A; RRID:AB_1264319 |
| anti-ZNF598, rabbit (1:1′000) | Bethyl Laboratories | Cat# A305-108A; RRID:AB_2631503 |
| anti-β-Actin, mouse | Sigma-Aldrich | Cat# A2228; RRID:AB_476697 |
| anti-FLAG, mouse (IF, 1:250) | Sigma-Aldrich | Cat# F1804; RRID:AB_262044 |
| anti-F9, mouse (IF, 1:600) | LSBio | Cat# LS-B6248; RRID:AB_10970782 |
| anti-RPL36a, mouse (1:1′000) | Santa Cruz Biotechnology | Cat# sc-100831; RRID:AB_2238666 |
| anti-S•Tag mouse, mouse (1:500) | Merck | Cat# 71549-3; RRID:AB_10806301 |
| IRDye® 800CW Donkey anti-Rabbit IgG (1:10′000) | LiCor | Cat# 926-32213; RRID:AB_621848 |
| IRDye® 680LT Donkey anti-Rabbit IgG (1:10′000) | LiCor | Cat# 926-68023; RRID:AB_10706167 |
| IRDye® 680LT Donkey anti-Mouse IgG (1:10′000) | LiCor | Cat# 926-68022; RRID:AB_10715072 |
| IRDye® 680LT Goat anti-Mouse IgG1-Specific (1:10′000) | LiCor | Cat# 926-68050; RRID:AB_2783642 |
| IRDye® 800CW Goat anti-Mouse IgG2a-Specific (1:10′000) | LiCor | Cat# 926-32351; RRID:AB_2782998 |
| Goat anti-Mouse IgG (H + L) Cross-Adsorbed Secondary Antibody, Alexa Fluor™ 488 (IF, 1:300 for S-tag AB detection and 1:500 for F9 antibody AB detection) | Invitrogen | Cat# A-11001; RRID:AB_2534069 |
| **Chemicals, peptides, and recombinant proteins** | | |
| Bortezomib | Merck | Cat# 504314 |
| Cycloheximide | Focus Biomolecules | Cat# 10-117 |
| MLN4924 (Pevonedistat) | Selleckchem | Cat# S7109 |
| Paromomycin | Sigma Aldrich | Cat# P5057 |
| Blasticidin S | Invitrogen | Cat# R21001 |
| Actinomycin D | Sigma-Aldrich | Cat# A9415 |
| CFTR inhibitor Inh172 | SigmaAldrich | Cat# C2292 |
| Geneticin (G418) | Thermo Fisher Scientific | Cat# BP673-5 |
| Puromycin | Sigma | Cat# P9620 |
| Lullaby | Oz Biosciences | Cat# LL71000 |
| DRAQ5™ (1:4′000) | Invitrogen | Cat# 65-0880-92 |
| Bovine Serum Albumin solution 35% in DPBS | Sigma-Aldrich | Cat# A7979 |
| Triton X-100 | Sigma-Aldrich | Cat# 93443 |

(*Continued on next page*)

*Continued*

| REAGENT or RESOURCE | SOURCE | IDENTIFIER |
|---|---|---|
| Polybrene | Sigma-Aldrich | Cat# TR-1003-G |
| Titanium Taq DNA polymerase and buffer | Clontech | Cat# NC9806143 |
| SPRI AMPure XL beads | Beckman Coulter | Cat# A63881 |
| Power SYBR green master mix | Thermo Fisher Scientific | Cat# A46012 |
| TRIS buffer | Qiagen | Cat# 19086 |
| Inh172 | Sigma-Aldrich | Cat# C2292 |
| Trypsin-EDTA (0.25%) | Gibco | Cat# 25200056 |
| PBS | Gibco | Cat# 10010001 |
| LightCycler® 480 Probes Master | Roche Diagnostic | Cat# 04707494001 |
| Gentamicin | Sigma-Aldrich | Cat #G1914 |
| T-Per protein extract solution | Thermo Fisher Scientific | Cat# 78510 |
| Protease inhibitors | Thermo Fisher Scientific | Cat# 78415 |
| Lysis buffer | Cell Signaling | Catt# 9803 |
| 4 to 12% Bis-Tris Polyacrylamide gels | Invitrogen | Cat# NW04122BOX |
| 4x NuPAGE LDS loading buffer | Thermo Fisher Scientific | Cat# NP0008 |
| Dynabeads™ Protein G | Invitrogen | Cat# 10004D |
| 1.5x LDS loading Bolt™ LDS Sample Buffer | Invitrogen | Cat# B0008 |
| RNase inhibitor | Vazyme | Cat# R301-3 |
| Micrococcal nuclease S7 | Thermo Fisher Scientific | Cat# EN0181 |
| EGTA | Thermo Fisher Scientific | Cat# 50-255-956 |
| DTT | Indofine Chemicals | Cat# MB1015 |
| Human iduronidase (IDUA; P35475) | Gentaur | Cat# MBS717919 |
| Endoproteinase AspN | Roche Diagnostic | Cat# 11054589001 |
| Iodoacetamide | Sigma-Aldrich | Cat# I1149-5G |
| Trypsin | Pierce | Cat# 90057 |
| Sequencing grade trypsin | Promega | Cat# V5111 |
| LysC | Promega | Cat# VA117A |
| T-Per permeabilization buffer | Thermo Fisher Scientific | Cat# 78510 |
| Protease Inhibitor cocktail EDTA free (100x) | Thermo Fisher Scientific | Cat# 78415 |
| Albumin | Pierce | Cat# 23209 |
| Cell Lysis Buffer (10X) | Cell Signaling | Cat# 9803 |
| 4-Methylumbelliferyl a-L-iduronide | Glycosynth | Cat# 44076 |
| 4-Methylumbelliferyl alpha-L-iduronic acid cyclohexylammonium salt | Gold Biotechnology | Cat# M570 |
| 4-Methylumbelliferyl beta-D-glucuronide | Sigma-Aldrich | Cat# M0130 |
| 4-Methylumbelliferone | Sigma-Aldrich | Cat# M1381 |
| Protease Inhibitor cocktail EDTA free (100x) | Thermo scientific | Cat# 78415 |
| Penicillin-Streptomycin (10,000 U/mL) | Invitrogen | Cat# 15140122 |
| FCS | Bioconcept | Cat# 2-01F16-I |
| L-Glutamine 200mM | Gibco | Cat# 25030149 |
| D-Saccharic acid-1,4-lactone SLM | Sigma-Aldrich | Cat# S0375 |
| Synthetic peptides | JPT Peptide Technologies | N/A |
| Lipofectamine™ RNAiMAX Transfection Reagent | Invitrogen | Cat# 13778075 |
| Lipofectamine™ LTX Reagent with PLUS™ Reagent | Invitrogen | Cat# 15338100 |
| Lipofectamine 2000 | Invitrogen | Cat# 11668019 |
| PLUS™ Reagent | Invitrogen | Cat# 11514015 |
| Opti-MEM | Gibco | Cat# 31985062 |
| LysC | Promega | Cat# VA117A |

(*Continued on next page*)

*Continued*

| REAGENT or RESOURCE | SOURCE | IDENTIFIER |
|---|---|---|
| HEPES | Invitrogen | Cat# 15630056 |
| 1x MEM Non-Essential Amino Acids Solution | Invitrogen | Cat# 11140035 |
| MEM (NEAA, no glutamine) | Gibco | Cat# 10370021 |
| Draq5 (Thermo Fisher Scientific, Cat# 62251) | Thermo Fisher Scientific | Cat# 62251 |
| Forskolin | Sigma-Aldrich | Cat# F6886 |
| siRNA pool GCN1 (+ control NegC) | siPool | Cat# 10985 |
| DMEM | Invitrogen | Cat# 41966052 |
| Luciferase expression | Promega | Cat# E2710 |
| Renilla-Glo™ reagent | Promega | Cat# E2710 |
| Paraformaldehyde | Electron Microscopy Sciences | Cat#15713-S |
| Cell stacks | Corning | Cat# 3319 |
| CaCl2 | Merck | Cat# 2382 |
| MgCl2 | Fluka | Cat# 63063 |
| FLIPR Blue VSD dye | Molecular Devices | Cat #R8034 |
| Transcriptor Universal cDNA Master | Roche Diagnostic | Cat# 05893151001 |
| Primer Probe Master - IDUA | Integrated DNA Technologies | Cat# Hs.PT.58.40058589 |
| Primer Probe Master - GAPDH | Integrated DNA Technologies | Cat# Hs.PT.39a22214836 |
| D-PBS | Invitrogen | Cat# 14190-144 |
| REF medium | Gibco | Cat# 11965092 |
| SperSignal™ West Femto Maximum Sensitivity Substrate | Thermo Fisher Scientific | Cat# 34096 |
| **Critical commercial assays** | | |
| Renilla-Glo assay substrate | Promega | Cat# E2750 |
| 660 nm Protein Assay | Pierce | Cat# 22660 |
| Blyscan Kit | Biocolor | Cat# B1000 |
| Pierce™ BCA Protein Assay Kit | Pierce | Cat# 23225 |
| Qiagen RNeasy Plus kit | Qiagen | Cat# 74134 |
| Qiagen's QIAamp DNA blood maxi kit | Qiagen | Cat #51194 |
| Quant-iT PicoGreen dsDNA assay | Invitrogen | Cat #P7589 |
| TruSeq SR Cluster v4 cBot kit | Illumina | Cat #GD-401-4001 |
| HiSeq SBS v4 50 cycle kit | Illumina | Cat #FC-410-1001 |
| RNeasy Plus kit | Qiagen | Cat# 74134 |
| Qubit Protein Assay | Invitrogen | Cat# Q33211 |
| **Deposited data** | | |
| SILAC-MS analysis | This study | Table S1 |
| eRF1-IP-MS analysis | This study | Table S2 |
| Genome-wide CRISPR and siRNA screens | This study | Table S3 |
| MS analysis of the polysome fractions | This study | Table S4 |
| MS raw data | (http://www.ebi.ac.uk/pride) | PXD042982 |
| **Experimental models: Cell lines** | | |
| IDUA W402X Hurler patient fibroblasts | Coriell | Cat# GM00798 (f) |
| IDUA Q70X Hurler patient fibroblasts | Telethon Foundation | Request-ID #834 |
| Jump-In™ HEK293 (HEKR4) | Thermo Fisher Scientific | N/A |
| Rat primary fibroblasts (REFs) | This study (NIBR) | N/A |
| HEKR4 GFP-CFTR-Y122X-Rluc | This study (NIBR) | N/A |
| HEKR4 GFP-CFTR-WT-Rluc | This study (NIBR) | N/A |
| HEKR4 F9-WT | This study (NIBR) | N/A |

(*Continued on next page*)

*Continued*

| REAGENT or RESOURCE | SOURCE | IDENTIFIER |
|---|---|---|
| HEKR4 F9-R338X | This study (NIBR) | N/A |
| HEKR4 CFTR | This study (NIBR) | N/A |
| HEKR4 CFTR PTC-Y122X | This study (NIBR) | N/A |
| HEKR4 CFTR PTC-G542X | This study (NIBR) | N/A |
| HEKR4 CFTR PTC-W1282X | This study (NIBR) | N/A |
| HEKR4 CFTR-S-tagged | This study (NIBR) | N/A |
| HEKR4 CFTR PTC-Y122X-S-tagged | This study (NIBR) | N/A |
| HEKR4 CFTR PTC-G542X-S-tagged | This study (NIBR) | N/A |
| HEKR4 CFTR PTC-W1282X-S-tagged | This study (NIBR) | N/A |
| HEKR4 RNF14_KO | This study (NIBR) | N/A |
| HEKR4 RNF14_KO_WT | This study (NIBR) | N/A |
| HEKR4 RNF14_KO_C220S (mut) | This study (NIBR) | N/A |
| HEKR4 RNF25_KO | This study (NIBR) | N/A |
| HEKR4 RNF25_KO_WT | This study (NIBR) | N/A |
| HEKR4 RNF25_KO_C135S/C138S (mut) | This study (NIBR) | N/A |
| Flp-In™ T-REx™ 293 Cell Line | Invitrogen | Cat# R78007 |
| Experimental models: Organisms/strains | | |
| Hurler IDUA-W401X rat | GenoWay (Lyon, France) | N/A |
| Sprague Dawley (SD) rat | This study (NIBR) | N/A |
| Oligonucleotides | | |
| For oligonucleotides, see Table S5 | This study | N/A |
| Recombinant DNA | | |
| pCRISPR (pU6-Esp3IgRNA-nlsSPYcas9nls-2apuroEGFP) | This study | N/A |
| pLenti6P-CMV-3xFLAG-NLS-SPyCas9_NLS-t2a-Hygro | This study | N/A |
| pJTI-R4-DEST CMV-pA (containig the sequences of the WT/PTC readthrough reporter or the coding sequences of CFTR, F9, IDUA and their corresponding mutants) | Thermo Fisher Scientific | N/A |
| pJTI™ R4 Int | Thermo Fisher Scientific | N/A |
| pcDNA3.1(+)-RNF14-WT-IRES-NTR | This study | N/A |
| pcDNA3.1(+)-RNF14-RM-IRES-NTR (ring mutant C220S) | This study | N/A |
| pcDNA3.1(+)-RNF25-WT | This study | N/A |
| pcDNA3.1(+)-RNF25-RM (ring mutant C135S, C138S) | This study | N/A |
| Software and algorithms | | |
| Inkscape | Inkscape | Software version 1.1.2 |
| GraphPad | GraphPad Software | Software version 9.0 |
| lightCycler480 | Roche Diagnostic | Software version 1.5.1.62 |
| MaxQuant | Max-Planck Institute of Biochemistry | Software version 1.3.0.5 |
| Chromeleon | Thermo Fisher Scientific | Software version 7.3.2 |
| Xcalibur | Thermo Fisher Scientific | Cat# OPTON-30965 |
| FragPipe | Nesvilab | Software version 1.8 |
| IonQuant | Nesvilab | Software version 1.8 |
| Biorender | Biorender | https://www.biorender.com |
| Other | | |
| ELISA assya plates | Greiner | Cat# 07-000-102 |
| 384 well black clear bottom black plate | Corning/Costar | Cat# 8742BC |

(*Continued on next page*)

*Continued*

| REAGENT or RESOURCE | SOURCE | IDENTIFIER |
|---|---|---|
| 384well black Poly-D-Lysin coated plates | BD Biocoat | Cat# BD359332 |
| Lysine coated 384well plates | Corning | Cat# 359332 |
| Lysine coated 384well clear bottom plates | Thermo Fisher Scientific | Cat# 142761 |
| 384well plates | Roche Diagnostic | Cat# 04729757001 |
| 384well plates | FrameStar | Cat# 4ti-0381/DBC |
| FrameStar®480, 384well PCR plate, white wells, clear frame | FrameStar | Cat# 4ti-0381/DBC |
| LightCycler® 480 System | Roche | Cat# 05015243001 |
| Roche Diagnostics LIGHTCYCLER 480 SEALING FOIL | Roche | Cat# 04729757001 |
| PHERAstar FSX plate reader | BMG LABTECH | Cat# PHERAstar FSX |
| Cellavista brightfield Imager system | Synetec | N/A |
| Automated cell culture device | SelecT, TAP_UK | N/A |
| 1536 well plate | Greiner | Cat# 789183-A |
| 1536 well black clear bottom plates | BD | Cat# 359315 |
| Envision reader | Perklin Elmer | Cat# 2105-0010 |
| Automated uHTS PinTool | Agilent | Cat# G5412-90002 |
| Flexdrop | Perklin Elmer | Cat# CLS155018 |
| uHTS Multidrop | Thermo Fisher Scientific | Cat# 5840330 |
| Acoustic Echo dispenser | Beckman | N/A |
| Series Acoustic Liquid Handler | Beckman | N/A |
| ViewLux uHTS Microplate Imager | PerkinElmer | Cat# 1430-0010A |
| FACS Aria | BD | N/A |
| Fluorescence microplate reader | Envision, Perkin Elme | Cat# 2105-0010 |
| cBot instrument | Illumina | Cat# SY-301-2002 |
| QiaShredder spin columns | Qiagen | Cat# 79654 |
| Roche LightCycler® 480 System | Roche Diagnostic | Cat# 05015243001 |
| FastPrep-24® Tissue and Cell homogenizer | MP Biomedicals | Cat# 116004500 |
| 1290 Infinity II LC System | Agilent | N/A |
| PHERAstar FSX plate reader | Bicolor | Cat# B1000 |
| iBlot 2 Dry Blotting System | Invitrogen | Cat# IB21001 and IB23001 |
| Trans-Blot Turbo Transfer System | Bio-Rad | Cat# 170415 |
| Sapphire Biomolecular Imager | Azure Biosystems | N/A |
| ChemiDoc XRS imaging device | Bio-Rad | N/A |
| Dual centrifugation using Zentrimix 380R | Hettich | Cat# 3220 |
| Gradient maker | BioComp | N/A |
| Ultracentrifuge tubes | Seton tubes | Cat# S7030 |
| SW 41 Ti rotor | Beckman Coulter | Cat# 331362 |
| Piston fractionator | BioComp | N/A |
| Spin columns | Pierce | Cat# 87777 |
| Dionex 3000 fitted with a 6.4 × 150 mm Zorbax C18 extend column | Thermo Fisher Scientific | N/A |
| Dionex, Ultimate 3000 | Thermo Fisher Scientific | N/A |
| LUMOS mass spectrometer | Thermo Fisher Scientific | N/A |
| NanoLC-MS/MS | Thermo Fisher Scientific | N/A |
| P-2000 laser puller | Sutter Instruments | Cat# P-2000 |
| ID fused silica | Dr Maisch Reprosil Pur120 | Cat# r13.aq. |
| Eksigent nanoLC | AB SCIEX | N/A |
| Hybrid LTQ-Orbitrap-Velos-Elite | Thermo Fisher Scientific | Cat# TSF-LTQ-OTEV-ETD |

(*Continued on next page*)

*Continued*

| REAGENT or RESOURCE | SOURCE | IDENTIFIER |
|---|---|---|
| Trapping column | Michrom Magi | N/A |
| 96-well microtiter plate format | Proxeon | Cat# CB080 |
| ICS3500 nano-UHPLC system | Thermo Fisher Scientific/Dionex | N/A |
| Easy spray column | Thermo Fisher Scientific | Cat# ES901 |
| QExactive | Thermo Fisher Scientific | Cat# IQLAAEGAA PFALGMBDK |
| (LC)-MS/MS | Thermo Fisher Scientific | N/A |
| Precolumn C18 PepMap100 | Thermo Fisher Scientific, Reinach, Switzerland | Cat# 160454 |
| C18 column | NYKKYO | Cat# NTCC-360/75-3-155) |

## RESOURCE AVAILABILITY

### Lead contact

Further information and requests for resources and reagents should be directed to and will be fulfilled by the lead contact, Oliver Mühlemann (oliver.muehlemann@unibe.ch).

### Materials availability

Plasmids and cell lines used in this study will be available upon request with a completed Materials Transfer Agreement.

### Data and code availability

- Four supplemental files contain the primary data of the SILAC-MS analysis (Tables S1), the eRF1-IP-MS analysis (Table S2), the genome-wide CRISPR and siRNA screens (Table S3), and the MS analysis of the polysome fractions (Table S4). The MS raw data has also been deposited in the PRIDE repository (http://www.ebi.ac.uk/pride) under the accession number: PXD042982.
- This paper does not report original code.
- Any additional information required to reanalyze the data reported in this work paper is available from the lead contact upon request.

## EXPERIMENTAL MODEL AND STUDY PARTICIPANT DETAILS

### Cell lines and culture conditions

The parental Jump-In HEK293 (Thermo Fisher Scientific, hereafter termed HEKR4) and all its derivatives were grown in medium containing DMEM (Invitrogen, Cat# 41966052), 10% dialyzed FCS (Bioconcept, Cat# 2-01F16-I), 25 mM HEPES (Invitrogen, Cat# 15630056), 1x MEM Non-Essential Amino Acids Solution (Invitrogen, Cat# 11140035), 100 units/ml of penicillin and 100 μg/mL of streptomycin (Invitrogen, Cat# 15140122), and 10 μg/mL Blasticidin S (Invitrogen, Cat# R21001). Primary patient fibroblasts homozygous for the IDUA W402X mutation were obtained from Coriell (GM00798 [female]; Deficient alpha-L-iduronidase; Hurler syndrome; homozygous for a TGG>TAG change at nucleotide 1293 in exon 9 of the IDUA gene [Trp402Ter (W402X)]) and fibroblasts homozygous for the IDUA Q70X mutation were provided by the Telethon foundation (Request-ID #834). These cells were cultured in medium containing MEM (NEAA, no glutamine, Gibco, Cat# 10370021) supplemented with, 2 mM L-Glutamine (Gibco, Cat# 25030149), 10% FCS (BioConcept, Cat# 2-01F16-I) and 100 units/ml of penicillin and 100 μg/mL of streptomycin (Invitrogen, Cat# 15140122). Rat primary fibroblasts (REFs) were grown in DMEM (Gibco, Cat# 11965092) containing 10% FCS, 100 units/ml of penicillin and 100 μg/mL of streptomycin (Invitrogen, Cat# 15140122). All cells were cultured at 37°C in humidified incubators with 5% $CO_2$. The NVS compounds, Bortezomib (BTZ, Merck, Cat# 504314), MLN4924 (Selleckchem, Cat# S7109) and Cycloheximide (CHX, Focus Biomolecules, Cat# 10–117) were all dissolved in DMSO, which also served as vehicle control. For long-term treatment up to 7 weeks in the patient and rat primary fibroblasts, the NVS compounds were reapplied every 3$^{rd}$ day with the medium change. Paromomycin (Sigma Aldrich, Cat# P9297) was dissolved in PBS.

### Engineering of recombinant PTC reporter, CFTR and IDUA cell models

Introduction of recombinant genes into the parental HEKR4 cell line was performed according to the manufacturer's guidelines (Thermo Fisher Scientific). In brief, HEKR4 contains a single R4 *attP* retargeting sequence and a promoterless Blasticidin resistance cassette ($Bsd^R$). To introduce a gene of interest (GOI) into the recombination site, the GOI was cloned into the pJTI-R4-DEST CMV-pA vector and co-transfected with the pJTI R4 Int vector for the expression of the integrase. $5x10^6$ cells per well of a 6-well plate were transfected with a mix of plasmid DNA, Lipofectamine LTX Reagent with PLUS Reagent (Invitrogen, Cat# 15338100) in Opti-MEM (Gibco, Cat#

31985062) according to the manufacturer's instructions. On the next day, the cells were transferred to T80 flasks and one day later, the growth medium was supplemented with 10 μg/mL Blasticidin S (Invitrogen, Cat# R21001) to select for site-specific integration events (positioning the EF1a promoter sequence in front of $Bsd^R$). After three weeks of culturing and Blasticidin selection, single cells were sorted into 96-well plates. Using the Cellavista brightfield Imager system (Syntec) for screening, single clones were identified and proliferated to the T80 format. While maintaining the Blasticidin selection for cell line propagation, the antibiotic was withdrawn from the medium 1–2 days prior to experimental procedures. For each of the integrated constructs, results from one cell clone are shown.

### Engineering of knockout and rescue cell lines

Candidate E3 ligases were knocked out using CRISPR-Cas9-mediated genome editing methods. Frist, the guide RNA sequences targeting exon 6 of RNF14 and exon 3 of RNF25 were inserted into the pU6-gRNA-SpyCas9-2A-Puro-eGFP plasmid using annealed oligonucleotides (see Key Resource Table) that were ligated into the Esp3I restriction sites. The resulting plasmid was used to transfect HEKR4 PTC reporter cells in 6-well plates with Lipofectamine 2000 (Invitrogen, Cat# 11668019) and PLUS Reagent (Invitrogen, Cat# 11514015) in Opti-MEM (Gibco, Cat# 31985062). After 24 h, the medium was supplemented with 2 μg/mL Puromycin (Sigma, Cat#P9620) to select for transfected Cas9 expressing cells (Cas9 is encoded as fusion protein with an $eGFP\text{-}Puro^R$ cassette intermitted by a P2A skipping sequence). Puromycin selection was maintained for 3 days and subsequently the cells were reseeded as single cell dilutions into 96-well plates. Clonal cell lines derived from single cells were then assessed for the loss of RNF14 and RNF25 expression by immunoblotting.

To reintroduce the E3 ligases in the background of the knockout cell lines, the open reading frames of RNF14 and RNF25 were PCR amplified and cloned into the pcDNA3.1(+) vector. For both E3 ligases, enzymatically inactive RING domain mutants were created (RNF14 C220S[44] and RNF25 C135S/C138S[45]). The resulting plasmids were transfected into RNF14 KO cells or RNF25 KO cells using Lipofectamine 2000 (Invitrogen, Cat# 11668019) and PLUS Reagent (Invitrogen, Cat# 11514015) in Opti-MEM (Gibco, Cat# 31985062). On the next day the growth medium was supplemented with 400 μg/mL Geneticin (G418, Thermo Fisher Scientific, Cat# BP673-5) to select for random genomic incorporation of the plasmids. Selection was maintained for about three weeks, before single cell-derived clones were raised for the RNF14 WT/mutant rescue cell lines as described above and assessed by immunoblotting. For the RNF25 WT/mutant rescue cell lines, protein overexpression was verified by immunoblot in the cell pools, which were then directly used for experiments. Blasticidin and G418 selection was maintained during cell line propagation and withdrawn from the medium 1–2 days prior to experimental procedures. Rluc readthrough measurements with RNF14, RNF25 KO and overexpressing cells was done as described in the HTS method section.

### Hurler IDUA-W401X rat model engineering and compound administration

CRISPR engineering and genetic analysis of the Wistar Kyoto Rat-W401X animal model was performed by GenoWay (Lyon, France). Breeding and karyotyping were outsourced to Charles River Laboratories (Wilmington, MA, USA) and Vium (San Mateo, CA, USA). Male and female animals homozygous for the IDUA W401X mutation were used at the age of 8–10 weeks (200–300 g weight) for NVS1.1 or NVS2.1 testing (IACUC: 15 DMP 067). Treatment and control groups (vehicle, WT untreated; n = 5) were separately housed. Vehicle solution and compound suspensions were prepared with 0.5% (w/v) Methylcellulose, Type 1500 in aqueous solution containing 0.5% (v/v) Polysorbate 80. Formulated NVS1.1 and NVS2.1 were stored at 2°C–8°C and protected from light. Animal weight was measured every third day and general health was monitored daily. Pharmacokinetics of NVS1.1 or NVS2.1 was determined from tail vein and terminal blood collections. Brain tissue compound concentration was determined from collected CSF fluid (see below). Tissues were snap frozen in liquid nitrogen and stored upon analysis.

The pharmacokinetic and pharmacodynamic studies in the Hurler rats were conducted between 2015 and 2018 and are documented under the reference number 120302 and the protocol number 15 DMP 067. The documents were approved by the Novartis animal welfare committee and the protocol 15 DMP 067 and all the subprotocols were approved by the IACUC under the title: Assessment of pharmacokinetics and pharmacodynamics properties of drug candidates in rats. Conducting and responsible Novartis scientists are the authors Mao Xiaohong and Juergen Reinhardt.

## METHOD DETAILS

### siRNA-mediated knockdown of GCN1

Approx. $4x10^6$ HEKR4 PTC reporter cells were grown on a 6-well plate and transfected with 40 nM of negative control (NegC, siPool) or GCN1 (siPool, 10985 – GCN1, human) targeting siRNA in a 200 μL serum-free mix containing 12 μL Lullaby (Oz Biosciences, Cat# LL71000), resulting in a final volume of 2 mL after addition to the cells. After one day, each condition was split 1:4 and one day later the transfection was repeated. One day after the second transfection the cells were treated with DMSO or 2.5 μM NVS1.1 for 6 h and immediately harvested by scraping in cold 1x PBS. The cells were then collected by centrifugation at 500 x *g* for 5 min at 4°C and stored at −80°C until further processing.

### High throughput screening and hit filtering

Screening (1.6 million compounds, 10 μM) was performed with the described HEKR4 GFP-CFTR-Y122X-hRluc cell line. Cell culture was supported by a fully automated cell culture device (SelecT, TAP_UK) and screening was done in 1536 well plate assay format

(Greiner, Cat. #789183-A). Cell passaging was done every 3rd. day and cell were used between cell passage 9–22. *Renilla* luciferase (RLuc) readout was carried out in a fully automated uHTS screening factory equipped with Envision (Perklin Elmer) readers. Cells were dispensed by the SelecT device (2′000 cells/well in 4 μL) and incubated for 24 h (37°C, 5% $CO_2$). Compounds were applied at a final concentration of 10 μM using an automated uHTS PinTool device (dispensing 40 nL compound solution per well). Control compound (paromomycin 14.4 mM f.c) was dispensed with a Flexdrop device to plate column 47 and 48. *Renilla*-Glo assay substrate (Promega, Cat. #E2750) was dispensed using an automated and customized uHTS Multidrop device (2.5 μL/well). Plates were slightly centrifuged at room temperature for 2 min on the screening factory. RLuc signal as readout for compound mediated translational readthrough was recorded with the Envision reader (0.1 s, US-Lum protocol, 0.1 mm distance aperture). Confirmation (20 μM, n = 4) and validation screening (n = 3, 8-point dose-response) was done offline using the very same readers. Offline compound transfer was done with an acoustic Echo dispenser (10–40 nL). Screening analysis and hit list selection was done with Novartis proprietary software. Z′ factor calculation was done with the formular Z' = 1–3* stdv High value) + 3* stdv (Low)/Average (High) – Average (Low) as previously described.[69] Screening hits were identified with the formular: A1 (%) = 100*(S-NC)/(AC-NC) where AC, NC and S correspond to Active Controls (injection of Stimulation buffer = 100% stimulation), Neutral controls (buffer injection $EC_{10}$) and screening samples (S). NC corresponds to 0% activity whereas AC is 100% activity (full stimulation). Post hit confirmation, screening hits were filtered with a HEKR4 GFP-CFTR-WT-Rluc cell line.

The compounds were triaged with an immunofluorescence imaging high content assay monitoring the restoration of the PTC mutant coagulation factor 9 (F9) R29X, stably expressed in HEKR4 cells. A corresponding F9-WT expressing HEKR4 cell line was used as reference. For AC (active control = 100%) control NVS2 was used. As screening neutral control (NC) DMSO solution (0.5% in media) was applied. Cell culture medium for F9 filtering was identical to the HTS Rluc assay. Compound transfer from compound source plates was done with an Echo device into 1536 well black clear bottom plates (BD Cat. #359315) containing 2′000 cells/well in 6 μL volume (cell media). Final compound concentration for confirmation screening was 10 μM (n = 4). For concentration response the compounds were diluted in 90% DMSO as 8-step dilution series and a dose range between 50 μM and 36 nM. For detection of F9 restoration paraformaldehyde-fixed (15 min, 4.4% f.c. in PBS) cells were washed twice with PBS, incubated with permeabilization and blocking solution (20% FCS, 0.2% Triton X-100 in PBS) for 30 min at room temperature and incubated with an anti-F9 antibody (1:600 in PBS, 1% FCS) together with a DRAQ5 (1:4′000) nuclear stain for 1 h at room temperature. Cells were washed with PBS and an anti-mouse IgG AF488 (1:300 in PBS, 1% FCS). Cells were washed twice with PBS and imaged (Opera imager) using dual excitation at 647 nm and 488 nm wavelength and emission at 690 nm and 549 nm for DARQ5 and antibody staining, respectively. IF data was analyzed with a proprietary imaging software. F9-containing cytoplasmic regions of interest were framed and nuclei imaging was excluded (% Factor IX + cells based passing the cytoplasmic intensity threshold). Z′ factor of the assay was >0.5.

### siRNA screen

HEKR4 PTC reporter cells grown as described above were used for the siRNA screen. The siRNA library, designed to target 19′300 genes whereby 8 different siRNAs were used per gene. siRNAs dissolved in Opti-MEM (Gibco, Cat# 31985062) were dispensed into 384 well plates, 75 nL/well using the Echo Series Acoustic Liquid Handler (Beckman) at room temperature. Lipofectamine RNAiMAX Transfection Reagent (Invitrogen, Cat# 13778075) was diluted 1:266 in Opti-MEM and 2 μL of this mixture was added to each well. Then 2 μL cell suspension containing 10′000 cells was transferred to each well. Finally, 10′000 cells (2 μL) were seeded into each transfection mix-containing well and incubated at 37°C, 5% $CO_2$ in humid atmosphere. One day later compound treatment was started by addition of NVS1.1 or NVS2.1 (3 μL/well) resulting in final concentrations of 1.21 μM or 6 μM, respectively which corresponds $IC_{80}$ of each compound to the previously determined in the recombinant cell models. DMSO was used as vehicle control. After 48 h of compound incubation, the luciferase expression was assessed (Promega, Cat# E2710) by addition of 3 μL Renilla-Glo reagent (Promega, Cat# E2710) and measuring the luminescence signal with the ViewLux uHTS Microplate Imager (PerkinElmer, Cat# 1430-0010A). The raw data was analyzed by a Novartis proprietary screening software as follows: Activity calculated as siRNA activity (Rluc) divided by median activity of plate negative control siRNA wells, Robust *Z* score normalization on each plate (robust *Z* score = (log2_FC – Median_Log2_FC)/(MAD_Log2_FC*1.4826). Statistical tests were performed using the RSA-analysis (redundance siRNA activity).[70]

### CRISPR screening procedures

CRISPR screen was done in GFP-CFTR-Y122X-Rluc reporter cells. Cas9 was stably expressed using the plasmid pLenti6P-CMV-3xFLAG-NLS-SPyCas9_NLS-t2a-Hygro. Stable cell clones were derived after 2 weeks of Hygromycin selection. Cas9 expression was confirmed by immunofluorescence with paraformaldehyde (4% f.c, 15 min, room temperature, Electron Microscopy Sciences, Cat. #15713-S) fixed cells. Blocking and antibody dilution was done in 3% bovine serum albumin (BSA) solution in DPBS (Sigma-Aldrich #A7979), 0.1% Triton X-100 (Sigma-Aldrich, Cat# 93443) solution in $H_2O$. The Cas9 protein contained an N-terminal FLAG tag to confirm expression (mouse anti-3x FLAG primary antibody, 1:250 dilution, RT, 3 h, Sigma-Aldrich Cat# F1804). Cells were washed with PBS buffer. The anti-FLAG antibody was detected using an anti-mouse Alexa 647 secondary antibody (Alexa 488 goat anti-mouse, 1:500 dilution, RT, 1 h, Invitrogen, #A11029). The images were captured with an InCell2000 imager.

### Cell line sensitivity to NVS1.1 and NVS2.1

Cells, $5x10^5$, were seeded into a 6 well format the day before compound addition. NVS1.1 was tested at 0, 1.5, 3, 6, 8 and 10 μM and NVS2.1 at 0, 6, 12, 24, 30 and 35 μM. The cells were incubated for 8 days with two changes of media containing the appropriate

compound concentration. Cell growth and death was monitored using microscopy imaging using GFP and bright field (BioRad ZOE Imager) and Cell TiterGlo. The final compound screening concentration was chosen at 3 μM for NVS1.1 and 24 μM for NVS2.1 (i.e., between 10 and to20-fold greater than the Reporter-RLuc $IC_{50}$ of each compound).

### Library transduction

For each compound screening two cell stacks (Corning, Cat# 3319) each containing $6.7x10^7$ of cells were seeded the day before virus infection. At the day of the infection, 700 mL cell culture medium per cell stack was completed with polybrene (8 μg/mL f.c.), mixed, incubated for 5 min before adding the calculated amount of virus stock (7 mL for C-pool 1 CP1004, 8 mL for C-pool 3 CP3001). The cell culture medium of the cell stacks was removed, and the virus-containing medium was poured into the cell stacks. The cell stacks were incubated at 37°C, 5% $CO_2$ for 24 h before exchanging the medium and adding puromycin-containing medium (4 μg/mL, final concentration). The transduction efficiency was monitored for five days post infection by RFP-positive cells measured by FACS Aria. Viral pools achieved >92% expression.

### Preparation of genomic DNA

Genomic DNA was prepared using Qiagen's QIAamp DNA blood maxi kit (Qiagen Cat #51194) as recommended by the manufacturer. The genomic DNA was eluted in 1 mL of buffer AE. To ensure complete recovery of the DNA, an extra 1 mL of buffer AE was added to the column and recovered again by centrifugation for 5 min.

*DNA quantification* Genomic DNA (gDNA) was quantified using the Quant-iT PicoGreen dsDNA assay (Invitrogen) following the manufacturer's recommendations. In short, the lambda DNA standard is diluted to a working concentration of 2 μg/mL using TE buffer. In an optically clear flat bottom 96 well plate a 10 point 100 μL volume lambda DNA standard curve is created by serially diluting the lambda DNA working solution using TE buffer. The gDNA is diluted in 100 μL TE buffer in an optically clear flat bottom 96 well plate. A working solution of PicoGreen is created by diluting the reagent 200-fold using TE buffer. 100 μL of the PicoGreen working solution is added to the lambda DNA standards and the diluted gDNA samples. The samples are mixed, incubated for 2–5 min at room temperature, protected from light and the fluorescence is measured using a fluorescence microplate reader (Envision, PerkinElmer) and standard fluorescein wavelengths following the manufacturer's recommendations. The gDNA sample concentration is then determined using the lambda DNA standard curve.

*Illumina library construction* To determine the gRNA representation of the lentiviral gRNA transduced samples (and the input gRNA plasmid library), the integrated gRNA sequences were PCR-amplified and sequenced using the Illumina sequencing technology. Illumina sequencing libraries are generated using PCR with primers specific to the integrated lentiviral vector sequence. PCR primers also contain additional sequences required for Illumina sequencing and sample multiplexing. It was empirically determined that a total of 96 μg of gDNA (an average of ~300 cells per gRNA), divided into 24, 4 μg PCR reactions, is required to accurately determined the representation of 55,000 gRNA sequences within a sample. PCR reactions are performed in a volume of 100 μL, containing a final concentration of 0.5 μM of each PCR primer (Integrated DNA Technologies, 5644 5′-AATGATACGGCGACCACCGAGATCTA CACTCGATTTCTTGGCTTTATATATCTTGTGGAAAGGA-3′ and INDEX 5′-CAAGCAGAAGACGGCATACGAGATXXXXXXXXXXGT GACTGGAGTTCAGACGTGTGCTCTTCCGATC-3′, where the X denote a 10 base PCR-sample specific barcode used for data demultiplexing following sequencing), 0.5 mM dNTPs, 1x Titanium Taq DNA polymerase and buffer (Clontech). PCR cycling conditions used are: 1 × 98°C for 5 min; 28 × 95°C for 15 s, 65°C for 15 s, 72°C for 30 s; 1 × 72°C for 7 min; and a final 4°C hold. The resulting Illumina libraries are purified using 1.8x SPRI AMPure XL beads (Beckman Coulter) following the manufacturer's recommendations. In short, 5 μL from eight independent PCR reactions are pooled together, generating three 40 μL pools (each pool containing eight PCR reactions). Each 40 μL pool is combined with 72 μL (1.8x) SPRI AMPure XL beads, mixed and incubated for 5 min at room temperature. Samples are then placed on a magnet (tube or plate) and left for 2 min at room temperature. The supernatant is carefully removed without dislodging the beads. The beads are washed with 200 μL fresh 75% ethanol for 30 s and the supernatant is carefully removed without dislodging the beads. The beads are air dried to remove any excess ethanol for 1–2 min at room temperature. Once dry, the samples are removed from the magnet, 50 μL of nuclease water is added, and the beads are mixed and incubated for 2 min at room temperature to elute the Illumina libraries from the beads. The samples are placed back on the magnet for 2 min and the supernatant is carefully removed into a new plate/tube without dislodging the beads.

*Illumina library quantification and pooling* The library pools are quantified using an SYBR green qPCR with primers specific to the Illumina sequences (Integrated DNA Technologies, P5 5′-AATGATACGGCGACCACCGAGA -3′ and P7 5′-CAAGCAGAAGACGGCA TACGA -3′). In short, 7.8 μL of Power SYBR green master mix (Thermo-Fisher), containing a final concentration of 2 μM of each primer (P5 and P7) is added to 7.2 μL of each library pool and subjected to qPCR; this is performed in duplicate. Additionally, a library of known concentration is run alongside as a control. qPCR cycling conditions used are: 1 × 95°C for 10 min; 30 × 95°C for 15 s, 60°C for 1 min. For the qPCR data analysis, a baseline of 2–8 $C_T$ and a threshold of 0.2 is used. $C_T$ values from technical duplicates are averaged and converted to a linear $C_T$ (LCT) value using the following equation LCT = Exp (average $C_T$ - 22.0)/−1.55). The library pools are then further pooled such that a total of four gDNA samples (i.e., 12 pools for 4 gDNA) are pooled for sequencing on one lane of an eight-lane high output HiSeq2500 sequencing flow cell. Pooling is done by pooling together a fixed LCT from each library pool. Each gDNA sample receives 50-60M reads which is equivalent to a ~1000 reads per sgRNA.

### Illumina flowcell generation and sequencing

For sequencing a single read HiSeq sequencing flowcell is prepared on the cBot instrument (Illumina), using a TruSeq SR Cluster v4 cBot kit (Illumina) and the 'SR_AMP_LIN_BLOCK_StripHyb.v9' cBot program, following the manufacturer's recommendations with the following changes. Library pools are denatured by combining 17 μL of 10mM TRIS buffer (Qiagen buffer EB) with 1 μL 2M NaOH and 2 μL of the 2000 LCT/μL library pools and incubated at RT for 5min. A 2 μL aliquot of the denatured library pool is then added to 1 mL of HT1 (Illumina), mixed and 120 μL is added to the 'sample library' cBot strip tube. As these libraries require a custom sequencing primer, reagent strip tube #2 in the cBOT reagent kit is replaced with a strip tube containing 350 μL per tube of a custom read 1 sequencing primer (Integrated DNA Technologies, 5645 5′-TCGATTTCTTGGCTTTATATATCTTGTGGAAAGGACGAAA CACCG-3′) at a concentration of 0.5 μM (e.g., 15 μL 100 μM 5645 primer in 3 mL HT1). The sample barcode is sequenced using the standard Illumina indexing primer (5′- GATCGGAAGAGCACACGTCTGAACTCCAGTCAC-3′), following the manufacturer's recommendations. The clustered flowcell is then sequenced with a 30b read 1 and an 11b index read using a HiSeq SBS v4 50 cycle kit (Illumina) following the manufacturer's recommendations.

### CRISPR screening

Due to toxicity of the lead compounds in this cell line it was possible to run this screen as a survival assay looking for genes that, when knocked-out by CRISPR-Cas9 indels, caused either increased sensitivity to the compounds (and hence causing these genes to be further under-represented in the pool of survivors) or alternatively to be lead to resistance to the compounds and hence to be over-represented in the pool of survivors. Live cells were collected after treatment and gDNA prepared for analysis of those genes over and underrepresented in the surviving pool.

### Hit analysis

After selection of cells surviving compound treatment, genomic DNA was prepared from the surviving cells and then used for sequencing and analysis of the barcoded CRISPR knockouts. Statistical tests were performed using the RSA-analysis (redundance siRNA activity).[70]

### CFTR expression assessment by immunofluorescence microscopy

HEKR4 cells stably expressing S-tagged wild type CFTR or the PTC mutants Y122X, G542X, W1282X were seeded in lysine coated 384-well plates (Corning, Cat# 359332), 8′000 cells/well. After 6 h, the cells were incubated with serial dilutions of NVS1 (0–25 μM), NVS2 (0–50 μM) or Paromomycin (0–10 mM). DMSO served as vehicle control. After 48 h, the anti-S tag antibody (Merck, Cat# 71549-3) was added directly to the medium of each well resulting in a final dilution of 1:500, followed by 20 min incubation at room temperature. Subsequently, the cells were fixed with 4% paraformaldehyde for 15 min at room temperature, followed by three washes with PBS. The primary antibody was then detected by an Alexa Fluor 488-conjugated goat anti-mouse secondary antibody (Invitrogen, Cat# A-11001), which was diluted 1:500 in blocking solution (PBS containing 1% FCS [Bioconcept, Cat# 2-01F16-I]) and incubated at room temperature for 1 h. DRAQ5 (Thermo Fisher Scientific, Cat# 62251) 1:5′000 diluted in 1% FCS was included in the same step to stain the nuclei of the cells. Cells were visualized with 20-63x magnification using the Zeiss LSMII confocal microscope.

### CFTR membrane potential assay

4′000 HEKR4 cells per well expressing the above-described CFTR variants were seeded into lysine coated 384 well clear bottom plates (Thermo Fisher Scientific, Cat# 142761). 6 h later, 10 μM NVS1 or NVS2, DMSO, or 10 mM Paromomycin was added (final concentrations), and cells were further incubated for 48 h in culture medium without antibiotics. Cells were then washed with a Na-Gluconate loading buffer containing 120 mM Na-Gluconate, 2 mM $CaCl_2$, (Merck, Cat# 2382), 2 mM $MgCl_2$ (Fluka, Cat# 63063), 10 mM HEPES, pH 7.4 at room temperature. The membrane potential dye was diluted as recommended by the manufacturer (Molecular Device, Cat# R8034) in loading buffer. After cell washing, 20 μL membrane potential dye in loading buffer was incubated in each well for 30 min at 37°C. 20 μM Forskolin (Sigma Aldrich, Cat# F6886, dissolved in ethanol) was injected online on an FLIPR (MD) high throughput cellular screening platform. Fluorescence increase was plotted as ΔF/Fb and normalized to the respective WT CFTR response. As a negative control, cells were preincubated for 20 min with 10 μM of the CFTR inhibitor Inh172 (Sigma-Aldrich, Cat# C2292) before Forskolin stimulation.

### RT-qPCR in Hurler patient-derived fibroblasts

Fibroblasts from a female Hurler syndrome patient (IDUA-W402X, Coriell Institute, Cat# GM00798) were grown in 6-well plates to a density of approx. $6x10^5$ cells per well. The cells were then incubated with different concentrations of NVS1.1 ranging from 0.3 μM to 5.0 μM for 8, 16, or 24 h. Thereafter, the cells were collected by trypsinization (Gibco, Cat# 25200056) and centrifugation for at 300 x *g* for 3 min at room temperature. After one wash with PBS (Gibco, Cat# 10010001), the cells were centrifuged as before, and the resulting cell pellet was snap frozen in liquid nitrogen and stored at −80°C. From the frozen cell pellet, total RNA was isolated using the Qiagen RNeasy Plus kit (Cat# 74134) according to the manufacturer's protocol with the following specifications: 200 μL Buffer RLT Plus was used for cell lysis, and homogenization was carried out using QiaShredder spin columns (Qiagen, Cat# 79654) including a centrifugation at 10′000 x *g* for 3 min at 4°C. The RNA concentration and purity were determined by measuring $A_{260}$ and $A_{260/280}$, respectively. Subsequently, cDNA was prepared using the Transcriptor Universal cDNA Master (Roche, Cat# 05893151001) in a

20 μL reaction containing 1x Transcriptor Universal Reaction Buffer, 1x Transcriptor Universal Reverse Transcriptase and 50 ng/μL total RNA, which was incubated at 29°C for 10 min (primer annealing), at 55°C for 10 min (reverse transcription) and at 85°C for 5 min (denaturation). The newly synthesized cDNA was then diluted to 10 ng/μL and stored at −20°C. The RT-control sample consisted of RNA diluted to the same final concentration. For the qPCR assay, the Roche LightCycler 480 System (Cat# 05015243001) in combination with 384-well plates (FrameStar, Cat# 4ti-0381/DBC, and Roche, Cat# 04729757001) was used. Each TaqMan qPCR reaction consisted of 1x LightCycler 480 Probes Master (Roche, Cat# 04707494001), 1x Primer Probe Master (predesigned assays for IDUA, Cat# Hs.PT.58.40058589 and GAPDH, Cat# Hs.PT.39a22214836 by Integrated DNA Technologies) and 2.5 ng/μL cDNA in a final volume of 10 μL and was run in the LightCycler480 (Software version 1.5.1.62) according to the manufacturer's guidelines. The relative mRNA levels were derived using the comparative $C_T$ calculation method.[71]

### Rat *in vitro and in vivo* studies

#### *Isolation of fibroblasts from Hurler IDUA-W401X rats*

Heterozygous knock-in rats were mated to produce pregnant heterozygous females. The dissected E13 embryo carcass was rinsed with cold D-PBS (Invitrogen cat# 14190-144) and dissociated in 1 mL 0.25% Trypsin-EDTA (Gibco, Cat# 25200056). After incubating in a humidified 5% $CO_2$ incubator at 37°C for ~2–3 min, 18 mL REF medium (DMEM [Gibco, Cat# 11965092] containing 10% FCS (Bioconcept, Cat# 2-01F16-I), 100 units/ml of penicillin and 100 μg/mL of streptomycin [Invitrogen, Cat# 15140122], Gentamicin [0.5mL], Sigma Cat. #G1914 was added to the digested tissues, followed by pipetting to dissociate the tissues. Dissociated tissues were transferred to tissue culture flasks, which were cultured at 37°C in a humidified 5% $CO_2$ incubator for several days until cells reached confluency. P0 rat embryonic fibroblast cells were passaged 2–3 times before compound testing.

### Brain tissue analysis

Frozen tissue samples were pulverized with a Covaris CP02 Cryoprep device according to the manufacturer's description. Pulverized samples were transferred in 2- or 15-mL matrix tubes, weighed and stored under ice. T-Per protein extract solution (Thermo Fisher Scientific, Cat# 78510) and protease inhibitors (Thermo Fisher Scientific, Cat# 78415) were added, vortexed and tubes were processed in a FastPrep-24 Tissue and Cell homogenizer as recommended by the manufacturer. Homogeneous liquid samples were stored on ice for 10 min. The process was repeated 3 times. Tissue samples were diluted to 1 g tissue/20 mL T-Per and centrifuged for 10 min. Supernatants were transferred, and all samples were stored at −80°C.

### Determination of the NVS1.1 and NVS2.1 concentration in the CSF

To determine the blood/CSF exposure ratio and time course, the concentrations of NVS1.1 or NVS2.1 in blood and CSF were measured from Sprague Dawley (SD) rats treated with a single peroral 10 mg/kg dose. NVS1.1 was dissolved in the standard MC/Tween80 suspension described above. For calibration of the mass spectroscopy analysis, NVS.1.1 and NVS2.1 dilutions from 0.1–10.000 ng/mL (n = 3) in artificial CSF fluid were used as standards. LC-MS analysis was done with an AB x 6500 and Agilent 1290 Infinity device. CSF sampling (20 μL) was done with the Cisterna Magna Cannulation method as described by others.[72] Compound concentrations in blood and CSF fluid (n = 3) were determined after various timepoints (0.25–24 h post dosing). The free plasma concentration was calculated based on NVS1.1 pharmacokinetic (PK) properties and determined plasma protein binding in rat.

### IDUA and GUSB enzyme assay

HEKR4 or primary fibroblast cells were seeded into black 384 well clear bottom plates (5000 cells/well) and incubated for 24 h at 37°C and 5% $CO_2$ in humid atmosphere before replacing the media with NVS compound-containing media further incubation for 48 h. For 7-day treatments, the compound-containing medium was exchanged after 3 days, and cells were incubated for an additional 4 days. Cell media was removed, and cells were lysed with 3 μL cold Lysis buffer (Cell Signaling, Cat. 9803) at 4°C under shaking. The IDUA enzyme substrate (4-Methylumbelliferyl α-L-Iduronide) and GUSB enzyme substrate (4-Methylumbelliferyl β-D-Glucuronide) were diluted as described by the manufacturer (Glycosynth). 5 μL of 0.4 mM of the respective substrate was added per well and incubated for 24–48 h at 37°C, 5% $CO_2$. The reaction was stopped with 40 μL glycine buffer (0.5 M glycine, 0.5 M $Na_2CO_3$, pH 10.2) and substrate fluorescence (360/450nm) was measured with a PHERAstar FSX plate reader. Enzyme activity was calculated as pmol or nmol per hour per mg total protein for IDUA and GUSB, respectively. Calibration curves were derived from fluorescence substrate dilutions. Sample protein concentration was measured with a BCA kit (Thermo Fisher Scientific, Cat# 23225). For brain tissue, IDUA activity determination 20–80 μg protein samples were used, whereas for the GUSB enzymatic measurements 20 μg protein samples were sufficient. The IDUA substrate was incubated for 48 h, whereas GUSB activity was measured after 30 min substrate addition.

### Total GAG assay

The Blyscan assay (Bicolor, Cat# B1000) is a quantitative dye-binding method for the analysis of sulfated proteoglycans and glycosaminoglycans (GAG). Total GAG from cell lysates and tissues was performed as described by the manufacturer and by others.[33] Reference standards and reagent blanks were used for calibration curves. Lysates were mixed with 1 mL dye reagent and incubated for 30–45 min at room temperature. Precipitates were centrifuged at 10′000 x *g* for 10 min and supernatant was removed. Deposits were dissociated with 0.5 mL dissociation reagent and extensively vortexed followed by an incubation of 30 min at room temperature.

Sample absorbance were measured with a microplate reader at appropriate wavelength. Plate or sample reading was done immediately. Determined GAG detection limit was 0.25 μg/sample. For brain tissue, a maximum volume of 100 μL with 300–400 μg protein/sample was used.

### Immunoblot

HEKR4 cell pellets were resuspended in RIPA buffer (50 mM Tris pH 8, 150 mM, 5 mM EDTA pH 8.0, 1% IGEPAL CA-630, 0.5% sodium deoxycholate, 0.1% SDS) and the lysate was isolated by centrifugation at 13′000 x *g* for 5 min at 4°C. After adjusting the protein concentrations in the lysates according to $A_{260}$, they were supplemented with 4x NuPAGE LDS loading buffer (Thermo Fisher Scientific, Cat# NP0008) to a final concentration of 1.5x and with 25 mM DTT. Of this, samples corresponding to approx. $5x10^4$ cell equivalents were loaded per lane. Samples deriving from whole cell lysates, immunoprecipitations or polysome fractionations were resolved on 4 to 12% Bis-Tris Polyacrylamide gels (Invitrogen, Cat# NW04122BOX, Cat# WG1401BOX and Cat# WG1403BOX) in MOPS buffer. Proteins were then transferred on nitrocellulose membranes using the iBlot 2 Dry Blotting System (Invitrogen, Cat# IB21001 and IB23001). The high molecular weight protein GCN1 was transferred using the Trans-Blot Turbo Transfer System (Bio-Rad, Cat# 1704150 and Cat# 1704158). Subsequently, the membranes were blocked with 5% milk in TBS containing 0.1% tween (TBS-t) and incubated with primary antibodies (dissolved in 5% BSA in TBS-t) for 2–3 h at room temperature or overnight at 4°C. After three washes with TBS-t, the membranes were incubated with IR-Dye-conjugated secondary antibodies (dissolved in 5% milk in TBS-t) for 1 h at room temperature. The membranes were washed again with TBS-t, dried and then scanned using the Sapphire Biomolecular Imager (Azure Biosystems). To assess eRF1 and beta-actin protein levels in compound treated fibroblasts (IDUA-W402X/Q70X Hurler patient-derived fibroblasts or rat IDUA-W401X fibroblasts) the immunoblot was performed analogously except for the usage of horseradish peroxidase (HRP)-conjugated secondary antibodies. HRP detection was carried out using the SuperSignal West Femto Maximum Sensitivity Substrate. The resulting signal was measured using a BioRad ChemiDoc XRS+ imaging device, quantified and normalized to the loading control beta-actin. For each experiment, results of at least two biological replicates are shown. All primary and secondary antibodies (along with their working concentrations) that were used in this study are listed in the Key Resource Table.

### Immunoprecipitation

For the pulldown of eRF1, one 15 cm dish of approximately 80% confluent HEKR4 PTC reporter cells was used for each condition. The cells were incubated with DMSO or 25 μM NVS1.1 for 30 min at 37°C, 5% $CO_2$ in humid atmosphere, immediately washed with cold 1xPBS and kept on a bed of ice. Subsequently, the cells were scraped off the plates in 1 mL cold 1x PBS, collected by centrifugation at 500 x *g* for 5 min at 4°C, and stored at −80°C until further processing. For the immunoprecipitation, cell pellets were thawed, resuspended in IP buffer (50 mM HEPES, pH 7.3, 600 mM NaCl, 0.5% Triton X-100), and cells were then lysed by dual centrifugation using Zentrimix 380R at 1500 rpm, for 4 min at −5°C. The resulting lysate was cleared by regular centrifugation at 16′000 x *g*, for 10 min at 4°C and the protein concentration was adjusted according to $A_{260}$. Before immunoprecipitation, 1/20 of the sample was combined with NuPAGE LDS loading buffer (Thermo Fisher Scientific, Cat# NP0008) to achieve a final concentration of 1.5x loading buffer and 25 mM DTT. The rest of the lysate was combined with 6 μg eRF1 antibody (Santa Cruz Biotechnology, Cat# sc-365686) coupled to 0.75 mg Dynabeads Protein G (Invitrogen, Cat# 10004D) for 1 h at 4°C under constant rotation. Subsequently, the beads were washed three times with IP buffer and the bound proteins were eluted in 1.5x LDS loading Bolt LDS Sample Buffer (Invitrogen, Cat# B0008) containing 25 mM DTT at 70°C for 10 min. For analysis by mass spectrometry, instead of eluting, the beads were washed three more times using IP buffer without detergent and stored at −20°C until further processing.

### Polysome fractionation

For each condition, HEKR4 PTC reporter cells were grown on 15 cm dishes to 80% confluency and incubated with either DMSO or 25 μM NVS1.1 for 30 min. Subsequently, the cells were treated with 100 μg/mL Cycloheximide (Focus Biomolecules, Cat# 10–117) and incubated for 4 min to stop translation and stabilize ribosomes on the mRNAs. After one wash with cold 1x PBS containing 100 μg/mL Cycloheximide, the cells were harvested by scraping them off the dish in the same buffer and collecting them by centrifugation at 500 x *g* for 5 min at 4°C. The cell pellets were resuspended in 300 μL lysis buffer containing 10 mM Tris-HCl pH 7.5, 10 mM NaCl, 10 mM $MgCl_2$, 1% Triton X-100, 1% sodium deoxycholate, 100 μg/mL Cycloheximide, 1 mM DTT and 0.1 u/μl RNase inhibitor (Vazyme, Cat# R301- 03) and incubated on ice for 2 min with occasional vortexing to ensure complete lysis. The resulting lysates were cleared by centrifugation at 16′000 x *g* for 5 min at 4°C and transferred into a new tube. Using the BioComp gradient maker, 15–50% sucrose gradients were formed in gradient buffer (10 mM Tris-HCl pH 7.5, 100 mM NaCl, 10 mM $MgCl_2$, 100 μg/mL Cycloheximide and 1 mM DTT) in ultracentrifuge tubes (Seton tubes, Cat# S7030), precooled at 4°C and balanced (+/− 0.01 mg). The lysates were loaded onto the sucrose gradients and centrifuged at 40′000 rpm for 2 h at 4°C using the SW 41 Ti rotor (Beckman Coulter, Cat# 331362). Subsequently, the gradients were fractionated into 1.5 mL tubes using the BioComp piston fractionator (volume displaced 0.143 mL/mm, scan speed 0.30 mm/s, distance 3.92 mm/fraction, 0.559 mL/fraction, start mode: meniscus sensing) and the $A_{260}$ profile was recorded. The retrieved fractions were then stored at −80°C. For protein analysis, the fractions were mixed with 1 volume of acetone and 0.1 volumes of 100% TCA, incubated overnight at −80°C, and the precipitated proteins were collected by centrifugation at 16′000 x *g* for 5 min at 4°C. Pellets were washed three times with ice-cold acetone (centrifugation as before), dried for 20 min in a SpeedVac and stored at −80°C. For immunoblot analysis, the protein pellet of every odd-numbered fraction was dissolved in

NuPAGE LDS loading buffer (Thermo Fisher Scientific, Cat# NP0008) to a final concentration of 1.5x and 25 mM DTT. 7% of the collected fraction was loaded per lane. For analysis by label-free mass spectrometry, 50% of two heavy polysome fractions (between fractions 16 and18, depending on the individual replicate) were pooled and precipitated as described above.

The polysome fractionations of nuclease treated lysate was performed as above with the following modifications: (1.) Cycloheximide was only added to the lysis buffer and not included into the PBS washes. (2.) Before loading the gradient, the lysate was digested with 400U Micrococcal nuclease S7 (Thermo Fisher Scientific, Cat# EN0181) in a reaction containing 1mM $CaCl_2$ for 45 min at 4°C followed by quenching with 1mM EGTA (Thermo Fisher Scientific, Cat# 50-255-956). (3.) Fractionation settings on the BioComp piston fractionator were: (i) volume displaced 0.16043 mL/mm, (ii) scan speed 0.30 mm/s, (iii) distance 3.92 mm/fraction, (iv) 0.559 mL/fraction, (v) start mode: slow-down distance. (4.) For immunoblotting (after precipitation), 10% of each fraction was loaded per lane.

### SILAC experiment in HEK293T cells to assess whole proteome changes under NVS1.1 treatment

HEK293T cells were metabolically labeled with heavy or light amino acids and treated for 24 h with 1 μM NVS1.1 or DMSO with swapping labels. Cells were harvested and pellets were resuspended in a buffer of 50 mM HEPES, 150 mM NaCl, 1.5 mM $MgCl_2$, and 1% SDS and lysed to completion by sonication with a probe tip sonicator. Samples were mixed in a 1:1 ratio according to protein concentration determined with the 660 nm Protein Assay (Pierce). A total protein input of approximately 20 μg was used per replicate experiment. Lysates were reduced with 10 mM DTT (Indofine Chemicals) at 30°C for 30 min, followed by alkylation with 25 mM iodoacetamide (Sigma-Aldrich) for 30 min at room temperature in the dark. Following SDS removal using detergent removal spin columns (Pierce, Cat# 87777), samples were digested overnight at 37°C with trypsin (Pierce, Cat# 90057) at a trypsin/protein ratio of 1:60, acidified with 5% formic acid and lyophilized. After resolubilization in separation buffer A (4% 5 mM ammonium formate, pH 10), in tryptic peptides were separated by high pH reversed-phase HPLC using a Dionex 3000 fitted with a 6.4 × 150 mm Zorbax C18 extend column with a flow rate of 1 mL/min. Eighty 1 mL fractions were collected throughout the segmented gradient (0–8% B/7 min, 8–27% B/38 min, 27–31% B/4 min, 31–39% B/8 min, 39–60% B/7 min, 60-0% B/20 min, separation buffer B: 96% acetonitrile, 4% 5 mM ammonium format, pH 10). After pooling to 17 fractions based on the UV absorption profile to achieve comparable peptide content per sample, the resulting fractions were analyzed by nanoLC-MS/MS. A nano LC column was prepared by creating a pulled tip with a P-2000 laser puller (Sutter Instruments) and packing the 75 μm ID fused silica with C18 material (Dr Maisch Reprosil Pur120, C18AQ 3 μm) to a length of 15 cm and fitted to the Eksigent nano \LC (AB SCIEX). The eluted peptides were reconstituted in 100 μL 2% acetonitrile in 0.1% formic acid (LC-MS Buffer A) and 25 μL was injected to the mass spectrometer (hybrid LTQ-Orbitrap-Velos-Elite, Thermo Fisher Scientific) using a trapping column (1 cm Michrom Magic C18AQ, 5 μm), washed for 20 min and then switched in-line with the analytical column. The peptides were eluted with a gradient of 3% LC-MS buffer B (70% acetonitrile in 0.1% formic acid) to 45% B in 80 min (0.5% B/min) delivered at a flow rate of 300 nL/min and using a top 20 CID analysis method with a dynamic exclusion set to 2. Data were analyzed with MaxQuant version 1.3.0.5 (Andromeda search engine with MaxQuant quantitation), searched against the UniProt Human database (V9 plus typical lab contaminants) with the addition of MaxQuant-generated reversed database to calculate false discovery rates. Database search criteria required full tryptic cleavage and allowed for up to 2 missed cleavages with oxidized methionine, and N-terminal acetylation as variable modifications and carbamidomethylation of cysteine as static modification. The results were visualized using GraphPad Prism.

### Determination of amino acid inserted at stop codon

#### *SDS-PAGE separation and in-gel digestion*

HEKR4 cells stably expressing IDUA-W402X with different stop codons (UAA, UAG or UGA) treated with 2 μM NVS1.1, 5 NVS2.1 or 14.4 mM Paromomycin for 24 h. The cells were then harvested, washed twice in PBS and after centrifugation at 250 x g for 5 min at 4°C resuspended in cell lysing buffer (Cell Signaling Cat# 9803, containing protease inhibitor, Thermo Fisher Scientific, Cat# 78415). Cell lysates were incubated on ice for 45 min with occasional mixing. Cell lysates were supplemented with LDS loading buffer containing 100 mM DTT. In parallel, a sample containing recombinant Human iduronidase (Gentaur, Cat# MBS717919) was prepared as reference. Separation of proteins was performed by SDS-PAGE using a NuPage Bis-Tris 4-12% gradient minigel (Invitrogen, Cat# NP0335) as described by the manufacturer. Approximately 0.3-0-8 μg of protein was applied to each gel lane. Three bands (approximately 1 mm) were typically excised between 70 and 80 kDa and further subjected to in-gel digestion.

In-gel digestion was performed as previously described[73] using a perforated 96-well microtiter plate format (CB080; Proxeon; DEN). Endoproteinase AspN (Roche Diagnostic, Cat# 11054589001) digestion of the gel pieces was performed in a 50 mM ammonium bicarbonate buffer (typically 240 ng of enzyme per sample)

### NanoLC-MS/MS - Parallel reaction monitoring (PRM)

Separation of peptides produced by AspN digestion was performed on a ICS3500 nano-UHPLC system (Thermo Fisher Scientific/Dionex, Germering, DE)) employing a 75 μm × 150 mm Easy spray column packed with C-18 reverse phase (Thermo Fisher Scientific, Cat# ES901) and a trapping column (Thermo Fisher Scientific, Cat# 164197). The column and trapping columns were kept at 40°C. Sample volumes of 5 μL were injected onto the trapping column. UPLC was controlled by Chromeleon software (Thermo Fisher Scientific). Eluent A was water containing 0.1% TFA. Eluent B was a 1:9 mixture of water: acetonitrile containing 0.09% TFA. A gradient from 20% B to 90% B was run in 60 min. The flow rate was typically 300 nL/min. The mass spectrometer was a QExactive (Thermo

Fisher Scientific) equipped with Easy-spray ESI source. Parallel reaction monitoring (PRM) was performed on the doubly charged ions from the target peptides of interest.[74] A list of 20 different target Asp-N digestion peptides containing the amino acid in position 402 of IDUA was monitored. Retention time and most abundant fragment information were obtained from LC-MSMS experiments using synthetic peptides from sequence $D_{397}$-$L_{412}$ (20 peptides each containing a different amino acid in position 402; see list in accessory records) Data were acquired and processed using the Excalibur software (Thermo Fisher Scientific). Semi-quantitative data were obtained from extracted ion intensities of peptide fragments.

### Label-free mass spectrometry for whole proteome and ubiquitination analysis

After immunoprecipitations, proteins associated with the Dynabeads were resuspended in 8 M urea, 50 mM Tris-HCl pH 8, reduced at 37°C for 30 min with 0.1 M DTT, 50 mM Tris-HCl pH 8, alkylated at 37°C for 30 min in the dark with 0.5 M iodoacetamide (IAA), 50 mM Tris-HCl pH 8, diluted with 4 volumes of 20 mM Tris-HCl pH 8 2 mM $CaCl_2$ prior to overnight digestion with 100 ng sequencing grade trypsin (Promega, Cat# V5111) at room temperature. Samples were then centrifuged, the magnetic beads trapped by a magnet, and the peptides-containing supernatant was collected.

The peptides were analyzed by liquid chromatography (LC)-MS/MS (PROXEON coupled to a QExactive HF mass spectrometer, Thermo Fisher Scientific) with three injections of 5 μL digests. Peptides were trapped on a μPrecolumn C18 PepMap100 (5μm, 100 Å, 300 μm × 5 mm, Thermo Fisher Scientific, Reinach, Switzerland, Cat# 160454) and separated by backflush on a C18 column (5 μm, 100 Å, 75 μm × 15 cm, C18, NYKKYO, Cat# NTCC-360/75-3-155) by applying a 60-min gradient of 5% acetonitrile to 40% in water, 0.1% formic acid, at a flow rate of 350 nL/min. The Full Scan method was set with resolution at 60,000 with an automatic gain control (AGC) target of 1E06 and maximum ion injection time of 50 ms. The data-dependent method for precursor ion fragmentation was applied with the following settings: resolution 15,000, AGC of 1E05, maximum ion time of 110 ms, mass window 1.6 m/z, collision energy 28, under fill ratio 1%, charge exclusion of unassigned and 1+ ions, and peptide match preferred, respectively.

For whole proteome analyses after polysome fractionations, cell pellets were re-suspended in 12 μL lysis buffer (8M Urea, 100 mM Tris-HCl pH 8, and a 1:10 dilution of 2 μL of the samples was used to measure protein concentration by Qubit Protein Assay (Invitrogen, Cat# Q33211). The remaining 10 μL were reduced, alkylated, and digested with LysC (Promega, Cat# VA117A) for 2 h at 37°C, followed by 100 ng Trypsin (Promega, Cat# V5111) overnight digestion at room temperature. The digests were analyzed by liquid chromatography on a Dionex, Ultimate 3000 (Thermo Fisher Scientific) coupled to a LUMOS mass spectrometer (Thermo Fisher Scientific) with two injections of 500 ng peptides.

The samples were loaded in random order onto a pre-column (C18 PepMap 100, 5 μm, 100 A, 300 μm i.d. x 5 mm length) at a flow rate of 10 μL/min with solvent C (0.05% TFA in water/acetonitrile 98:2). After loading, peptides were eluted in back flush mode onto a homemade pack C18 CSH Waters column (1.7 μm, 130 Å, 75 μm × 20 cm) by applying a 90-min gradient of 5%–40% acetonitrile in water, 0.1% formic acid, at a flow rate of 250 nL/min.

Data acquisition used the data dependent mode, with precursor ion scans recorded in the orbitrap with resolution of 120′000 (at m/z = 250) parallel to top speed fragment spectra of the most intense precursor ions in the linear trap for a cycle time of max. 3 s.

Peptides and proteins were searched and quantified using FragPipe version 1.8.[75–77] A closed search was performed with the Swissprot[78] human database containing isoforms (release June 2022), to which reverse decoys and common contaminants were added. Fragment mass tolerance was set to 20 ppm for IP samples and to 0.4 Da for samples from lysed cells, respectively. Search enzyme was set to "strict trypsin" and allowed missed cleavages to 3. Carbamidomethylation was set as a fixed modification on cysteine, and the following variable modifications were enabled: methionine oxidation, ubiquitination residue on Lysine and protein N-terminal acetylation. Philosoper's peptide and protein prophet[75] were selected, respectively, for filtering and protein inference with default parameters, and IonQuant[77] for quantification. Match between runs was enabled, with top runs set to 2 for the beads study and 3 for the protein pellets study.

Differential protein expression was determined as follows: Protein groups with only 1 peptide evidence and the common contaminants were removed. Imputation was performed if there were at least 2 detections in at least one group of replicates. If there was at most 1 non-zero value in the group for a protein, then the remaining missing values were imputed by drawing values from a Gaussian distribution of width 0.3 times the sample standard deviation and centered at the sample distribution mean minus 2.5 times the sample standard deviation. Any remaining missing values were imputed by the Maximum Likelihood Estimation[79] method. Differential expression by moderated t statistics between the two groups and significance evaluation was performed as previously described.[80] The relative modification degree for ubiquitination residues was obtained by first summing the contributing intensities to each ubiquitination site in each sample, then dividing this quantity by the protein intensity, and averaging the result across the replicates.

## QUANTIFICATION AND STATISTICAL ANALYSIS

All data are presented as mean ± standard deviation (SD) from at least three independent biological experiments or samples. Statistical analyses were performed using GraphPad Prism 9. *p* values were calculated by one-way ANOVA followed by Dunnet's multiple comparisons test. *p* values of $\leq 0.05$, $p \leq 0.01$, and >0.05 are depicted as *, **, and ns (non-significant), respectively. Hit analysis, siRNA screen, and the gene significance statistical tests were performed using the RSA-analysis (redundance siRNA activity). The statistical test for label-free mass spectrometry for whole proteome and ubiquitination analysis was conducted using moderated t statistic. See method details and figure legends for detailed information.

**Cell Reports, Volume *42***

## Supplemental information

# Drug-induced eRF1 degradation promotes readthrough and reveals a new branch of ribosome quality control

**Lukas-Adrian Gurzeler, Marion Link, Yvonne Ibig, Isabel Schmidt, Olaf Galuba, Julian Schoenbett, Christelle Gasser-Didierlaurant, Christian N. Parker, Xiaohong Mao, Francis Bitsch, Markus Schirle, Philipp Couttet, Frederic Sigoillot, Jana Ziegelmüller, Anne-Christine Uldry, Wojciech Teodorowicz, Niko Schmiedeberg, Oliver Mühlemann, and Jürgen Reinhardt**

## Supplemental information

# Drug-induced eRF1 degradation promotes readthrough and reveals a new branch of ribosome quality control

Lukas-Adrian Gurzeler, Marion Link, Yvonne Ibig, Isabel Schmidt, Olaf Galuba, Julian Schoenbett, Christelle Gasser-Didierlaurant, Christian N. Parker, Xiaohong Mao, Francis Bitsch, Markus Schirle, Philipp Couttet, Frederic Sigoillot, Jana Ziegelmüller, Anne-Christine Uldry, Wojciech Teodorowicz, Niko Schmiedeberg, Oliver Mühlemann and Jürgen Reinhardt

Content of this file:

- Figures S1 to S6
- Table S5

Additional supplemental information provided as separate files:

- Table S1. MS-SILAC data, NVS1.1 versus DMSO (CSV file)
- Table S2. MS of eRF1 IP, di-Gly analysis, NVS1.1 versus DMSO (XLSX file)
- Table S3. CRISPR and siRNA screens, NVS1.1 and NVS2.1 hit list (CSV file)
- Table S4. MS of polysome fractions, NVS1.1 versus DMSO (XLSX file)

# Figure S1

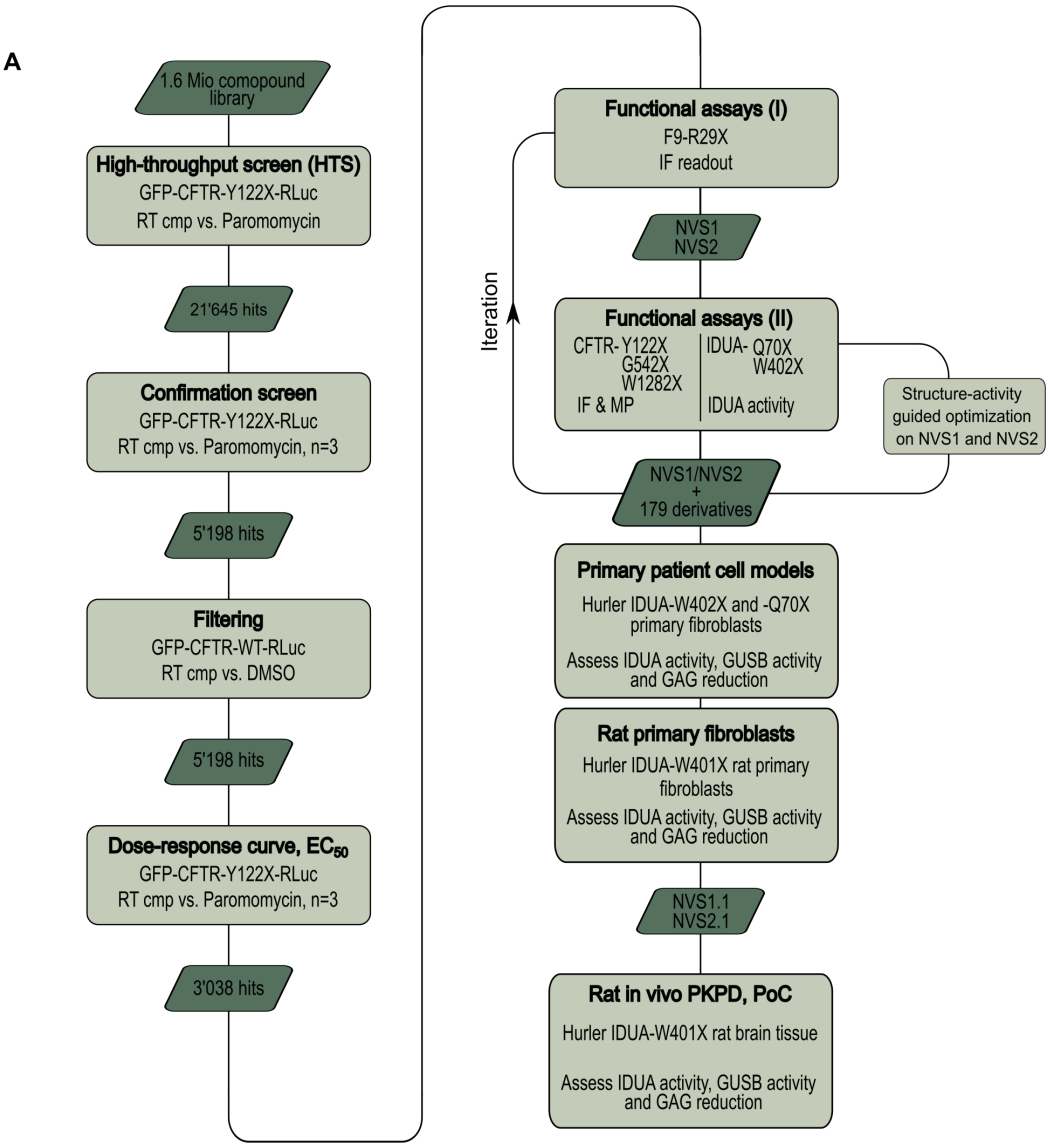
A
1.6 Mio comopound library
High-throughput screen (HTS)
GFP-CFTR-Y122X-RLuc
RT cmp vs. Paromomycin
21'645 hits
Confirmation screen
GFP-CFTR-Y122X-RLuc
RT cmp vs. Paromomycin, n=3
5'198 hits
Filtering
GFP-CFTR-WT-RLuc
RT cmp vs. DMSO
5'198 hits
Dose-response curve, EC50
GFP-CFTR-Y122X-RLuc
RT cmp vs. Paromomycin, n=3
3'038 hits
Iteration
Functional assays (I)
F9-R29X
IF readout
NVS1
NVS2
Functional assays (II)
CFTR- Y122X G542X W1282X
IF & MP
IDUA- Q70X W402X
IDUA activity
Structure-activity guided optimization on NVS1 and NVS2
NVS1/NVS2 + 179 derivatives
Primary patient cell models
Hurler IDUA-W402X and -Q70X primary fibroblasts
Assess IDUA activity, GUSB activity and GAG reduction
Rat primary fibroblasts
Hurler IDUA-W401X rat primary fibroblasts
Assess IDUA activity, GUSB activity and GAG reduction
NVS1.1
NVS2.1
Rat in vivo PKPD, PoC
Hurler IDUA-W401X rat brain tissue
Assess IDUA activity, GUSB activity and GAG reduction

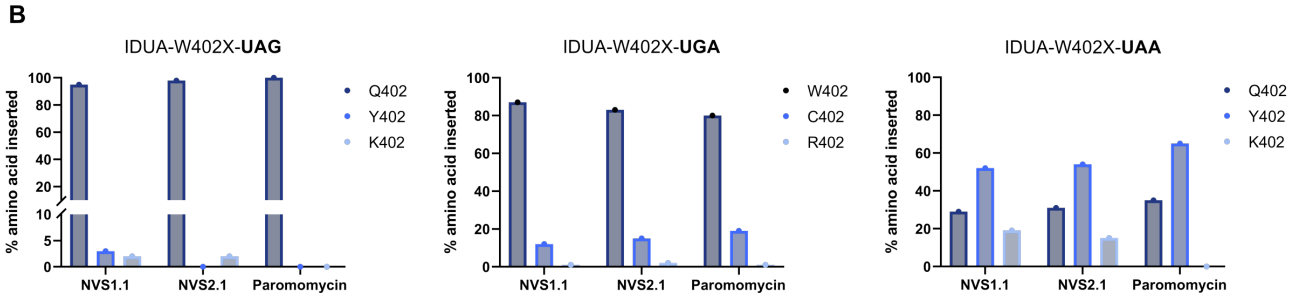
B
IDUA-W402X-UAG
% amino acid inserted
Q402
Y402
K402
NVS1.1
NVS2.1
Paromomycin
IDUA-W402X-UGA
W402
C402
R402
IDUA-W402X-UAA

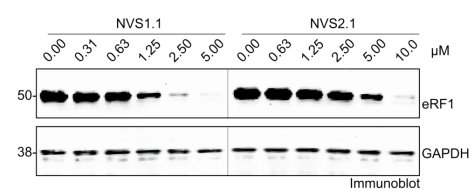
C
NVS1.1
NVS2.1
0.00
0.31
0.63
1.25
2.50
5.00
10.0
µM
50
eRF1
38
GAPDH
Immunoblot

**Figure S1, related to Figure 1. Flowchart of the high-throughput screen for readthrough-promoting drugs, identification of amino acids inserted at the different termination codons, and documentation of eRF1 depletion induced by NVS1.1 and NVS2.1.**

(A) Flowchart depicting the lead compound identification and triaging of positive hits. Abbreviations: Half maximal effective concentration ($EC_{50}$), immunofluorescence (IF), membrane potential (MP), proof of concept (PoC).

(B) Quantitative Nano-LC-MS/MS to determine the incorporated amino acid at each of the three TCs in recombinant W402X-IDUA expressing HEKR4 cells in response to NVS1.1, NVS2.1 or Paromomycin. The bars show the percentage of insertion of the indicated amino acids among all detected readthrough events.

(C) Immunoblot analysis of the eRF1 abundance after treatment of HEKR4 cells with serial dilutions of NVS1.1 or NVS2.1 for 6 h. GAPDH protein levels were assessed as loading control.

# Figure S2

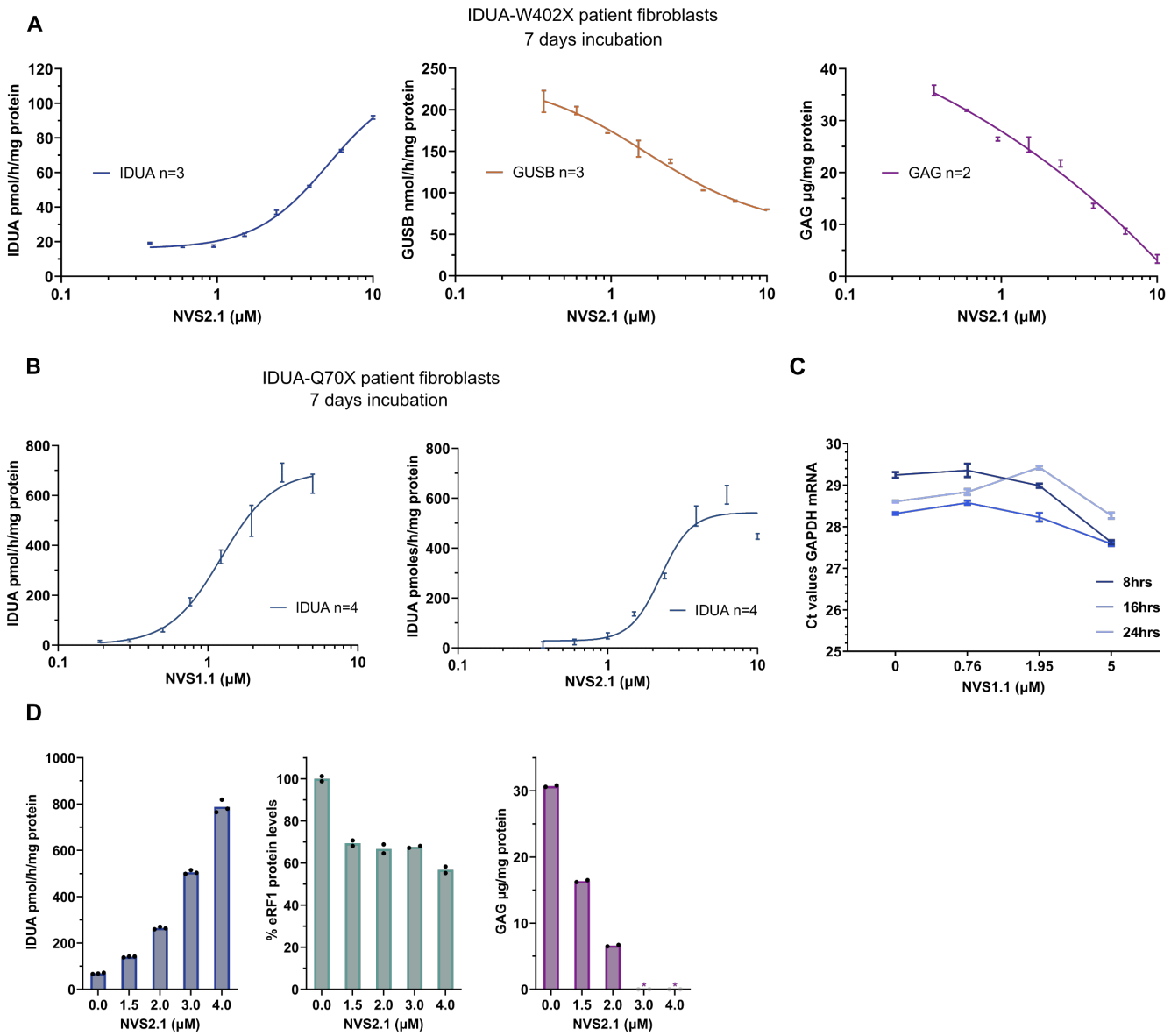


**Figure S2, related to Figure 2. NVS2.1 and NVS1.1 restore α-L-iduronidase in Hurler patient-derived fibroblasts at concentrations that do not yet inhibit NMD.**

(A) Primary fibroblasts deriving from patients homozygous for the IDUA W402X mutation were treated for 7 days with the indicated concentrations of NVS2.1. Subsequently, α-L-iduronidase (IDUA) and β-glucuronidase (GUSB) activities were assessed by measuring the conversion rates of the surrogate substrates 4-Methylumbelliferyl-α-L-iduronide (pmol/h/mg protein) and 4-Methylumbelliferyl-β-D-glucuronide (nmol/h/mg protein), respectively. Total glycosaminoglycan (GAG) levels were determined by a colorimetric assay and normalized to total protein abundance (GAG, µg/mg protein). Mean values ± SD are shown.

(B) Primary Hurler patient fibroblasts homozygous for the IDUA Q70X mutation were cultured for 7 days in the presence of NVS1.1 or NVS2.1 (compound exchange every 3$^{rd}$ day) and α-L-iduronidase enzymatic activity was assessed as in (A). Mean values ± SD are shown.

(C) RT-qPCR assay showing the GAPDH mRNA Ct (cycle threshold) values upon treatment of the Hurler primary fibroblasts with different concentrations of NVS1.1 for 8 – 24 hours. Mean values ± SD are shown (n=3).

(D) Primary Hurler IDUA-W402X fibroblasts were cultured in different concentrations of NVS2.1 with medium and compound exchange every 3$^{rd}$ day. After 7 weeks, the IDUA activity and total GAG levels were determined as in (A). Asterisks denote GAG measurements below the assay detection limit. The eRF1 protein abundance was assessed by immunoblot (using β-actin as a loading control) and is expressed relative to the DMSO-treated control condition.

# Figure S3

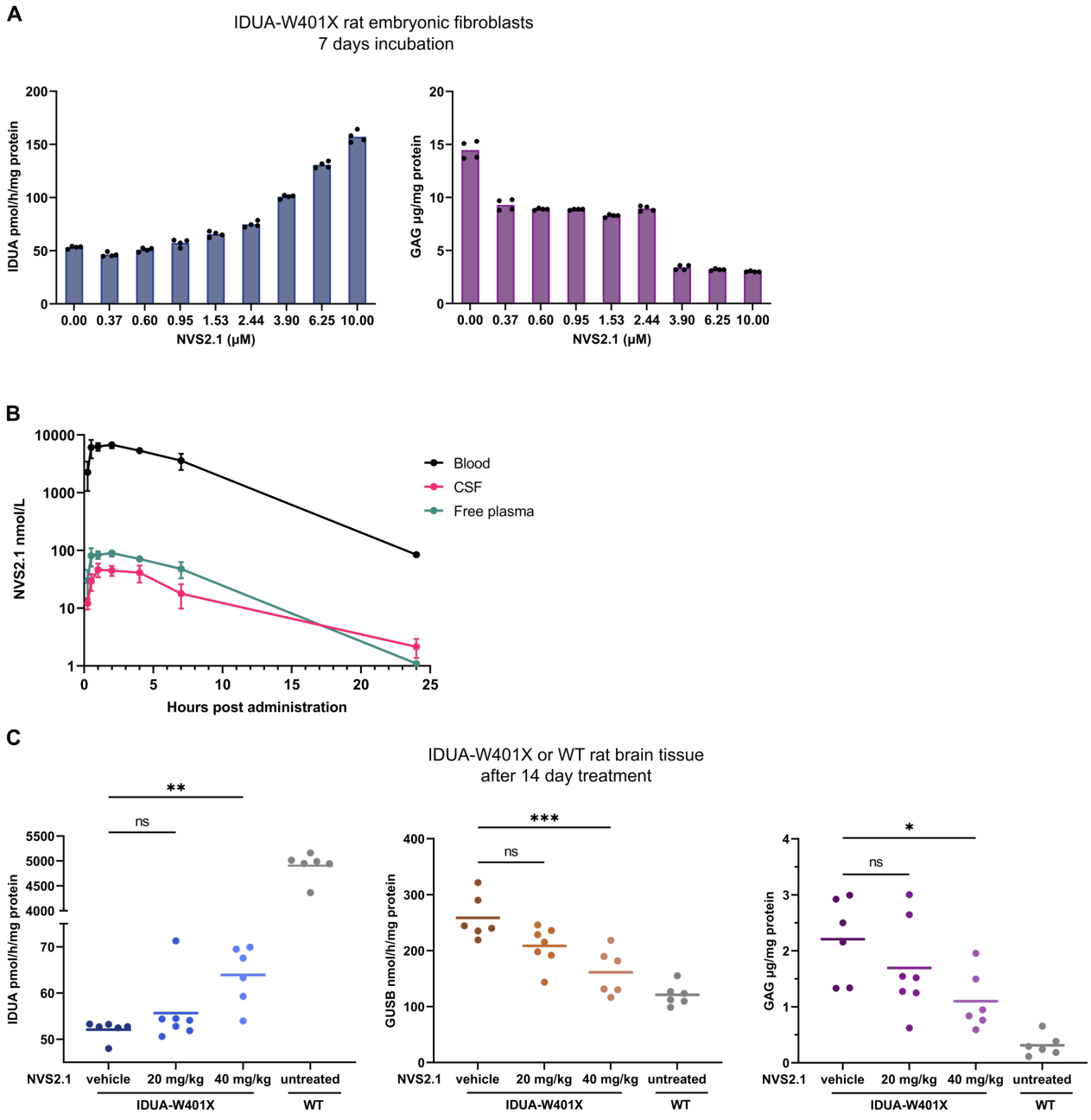


**Figure S3, related to Figure 3. NVS2.1 reduces the glucosamine load in the brain of a rat Hurler disease model.**

(A) Freshly isolated rat fibroblasts of a Hurler animal model homozygous for IDUA-W401X were treated for 7 days with different concentrations of NVS2.1. The IDUA enzyme activity and total GAG levels were determined as in Figure S2A.

(B) NVS2.1 concentrations (nmol/L) were determined in total blood and cerebrospinal fluid (CSF), and calculated for free plasma, at different timepoints after a single oral administration of 10 mg/kg NVS2.1 to male Sprague Dawley (SD) rats (n=3). Mean values ± SD are shown.

(C) Rats homozygous for the IDUA W401X mutation were treated with 20 mg/kg (n=7) or 40 mg/kg (n=6) NVS2.1, or with the vehicle formulation only (n=6) for 14 days. A similar number of untreated animals with WT IDUA was analyzed for comparison. After scarifying the animals, the brain tissue was extracted and the activities of IDUA and GUSB along with the total GAG levels were determined as in Figure S2A. In each graph (IDUA, GUSB, GAG), one dot represents the average of four technical replicates carried out with brain tissue from one animal. *P* values were calculated by one-way ANOVA followed by Dunnet's multiple comparisons test. *P* values of ≤ 0.05, p≤ 0.01, p≤ 0.001 and >0.05 are depicted as *, **, ***, and ns (non-significant), respectively.

## Figure S4

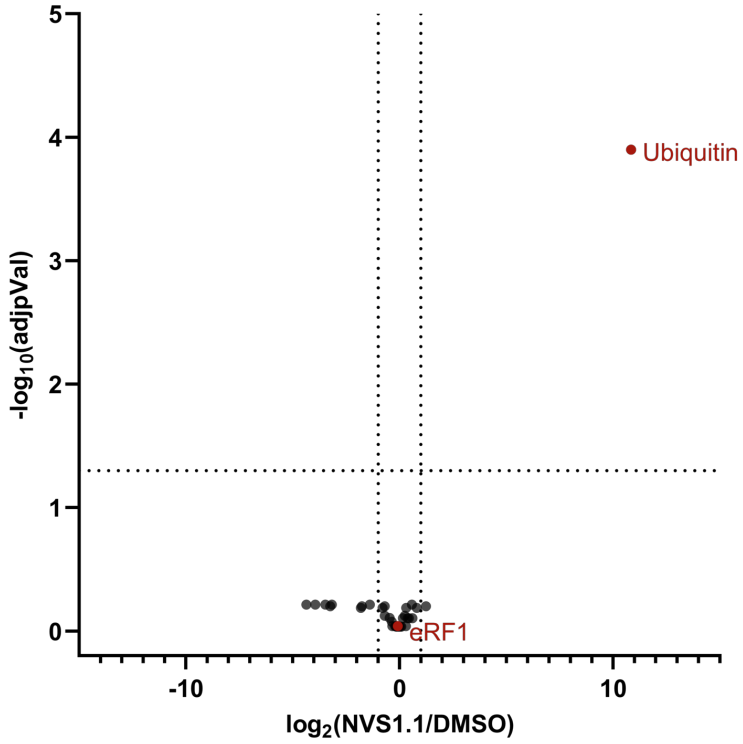


**Figure S4, related to Figure 4. NVS1.1 induces eRF1 ubiquitination.** Label-free mass spectrometry analysis depicting the fold change of identified proteins upon treatment with NVS1.1 ($log_2$(NVS1.1/DMSO), x-axis), versus its statistical significance ($log_{10}$adjp-value, y-axis) of the immunoprecipitates of Figure 4B.

# Figure S5

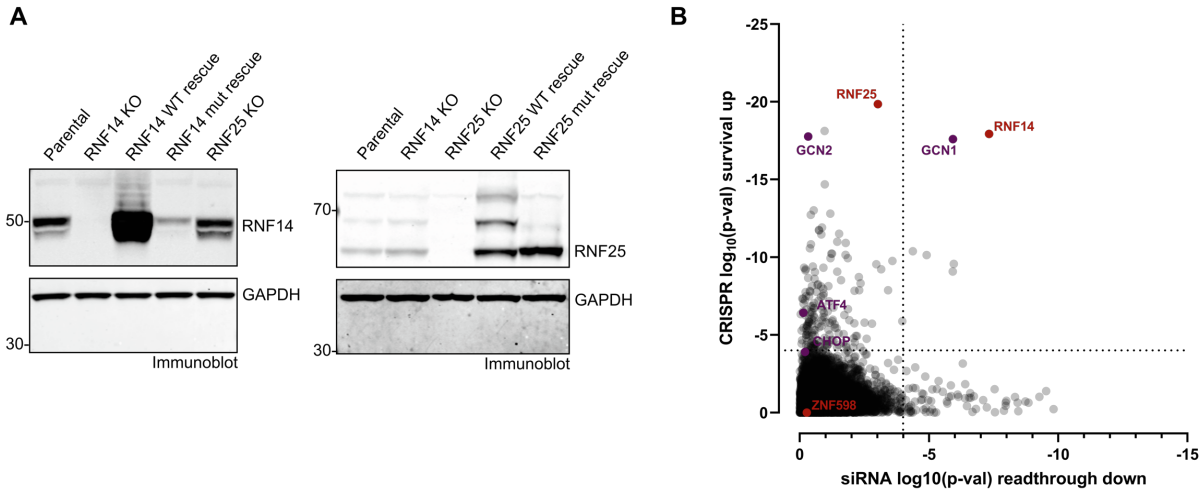


**Figure S5, related to Figure 5. Assessment of RNF14 and RNF25 protein levels in the respective knockout and rescue cells, and identification of factors involved in NVS2.1-mediated translational readthrough.**

(A) Detection of the RNF14 and RNF25 protein levels in the knockout and rescue cell lines by immunoblotting. GAPH served as a loading control.

(B) Combined results of a genome-wide siRNA screen scoring for reduced NVS2.1-mediated readthrough and a CRISPR knockout screen enriching for genes leading to NVS2.1 resistance. X-axis: $\log_{10}$ p-values depicting the significance of the reversion of NVS2.1-induced readthrough in CFTR-Y122X-Rluc reporter gene expressing HEKR4 PTC cells for the knockdown of each of the 19'300 tested genes. For each gene knockdown (8 siRNAs per gene), Rluc activity was normalized to the luminescence signal of a non-targeting siRNA ($\log_2$FC) and the differential activity between the two treatment conditions (NVS2.1 $IC_{80}$ vs. DMSO) was determined. The gene significance was calculated for the differential activity of each gene knockdown using the RSA statistical test (redundance siRNA activity; Konig et al., *Nat Methods* 4(10):847-9, 2007). Y-axis: $\log_{10}$ p-values depicting the significance of the reversion of NVS2.1-induced toxicity in a cell survival assay for the knockout of each of the 19'300 tested genes. Differential representation of each sgRNA in NVS2.1 $IC_{80}$ and untreated library-infected cell populations was determined as surrogate of difference in cell proliferation. The gene significance was calculated for the differential representation of each sgRNA set (5 sgRNAs per gene) using the RSA statistical test. For both screens, the significance thresholds were determined by randomizing the gene labels before running the RSA tests. A $\log_{10}$(p-Val) <-4 threshold (dotted lines) limited false positives to ~5%.

# Figure S6

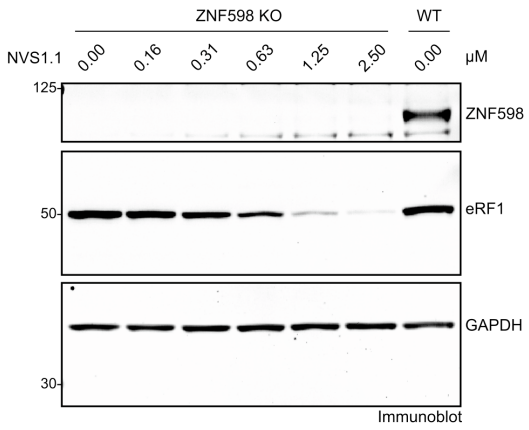


**Figure S6, related to Figure 6. ZNF598 is not required for NVS1.1-mediated eRF1 depletion.**

HEK Flp-In T-REx cells containing a ZNF598 knockout (ZNF598 KO) were incubated with NVS1.1 for 6 h and analyzed for eRF1 by immunoblot using GAPDH as normalizer. In addition, lysate of untreated HEK cells was loaded to confirm the depletion of ZNF598 on the immunoblot.

**Table S5. TaqMan assay information, and sequences of oligonucleotide used for generating RNF14 and RNF25 knockouts and libraries for Illumina sequencing.**

| Oligonucleotides | | |
|---|---|---|
| Name | Sequence 5'-3' or identifier | Supplier |
| IDUA TaqMan assay | Cat# Hs.PT.58.40058589 | Integrated DNA technologies |
| GAPDH TaqMan assay | Cat# Hs.PT.39a22214836 | Integrated DNA technologies |
| sgRNA_RNF25_fwd | accgACCCTCTAGATGTAGTGAAA | - |
| sgRNA_RNF25_rev | aaacTTTCACTACATCTAGAGGGT | - |
| sgRNA_RNF14_fwd | accgGTGCAGGTTGACCTACCATG | - |
| sgRNA_RNF14_rev | aaacCATGGTAGGTCAACCTGCAC | - |
| 5644 | AATGATACGGCGACCACCGAGATCTACACTCGATTTCTTGGCTTT ATATATCTTGTGGAAAGGA | Integrated DNA technologies |
| INDEX | CAAGCAGAAGACGGCATACGAGATXXXXXXXXXXGTGACTGGAG TTCAGACGTGTGCTCTTCCGATC | Integrated DNA technologies |
| P5 | AATGATACGGCGACCACCGAGA | Integrated DNA technologies |
| P7 | CAAGCAGAAGACGGCATACGA | Integrated DNA technologies |
| 5645 | TCGATTTCTTGGCTTTATATATCTTGTGGAAAGGACGAAACACCG | Integrated DNA technologies |